UNIVERSITY OF CALIFORNIA

Los Angeles

Mussel-inspired elastic bioadhesives with hemostatic andantimicrobial properties for wound healing

A thesis submitted in partial satisfaction of the requirements for the degree

Master of Science in Chemical Engineering

by

Saumya Jain

2022

ABSTRACT OF THE THESIS

Mussel-inspired elastic bioadhesives with hemostatic and antimicrobial properties for wound healing

by

Saumya Jain

Master of Science in Chemical Engineering

University of California, Los Angeles, 2022

Professor Nasim Annabi, Chair

Traumatic injury is a leading cause of death worldwide whose treatment process is riddled with medical complications including hemorrhage and infection. Biomaterials that have recently been developed for wound treatment often neglect to take these hurdles into account or lack important characteristics, such as biocompatibility, biodegradability, and adhesion to bleeding tissue surfaces. In this work, we synthesized a multifunctional gelatin-based hydrogel for hemorrhage control that retained mechanical characteristics suitable for use on dynamic and elastic surfaces such as skin or motive internal organs such as lungs and heart. The designed multifunctional hydrogel also exhibited robust adhesion to wet tissue surfaces, strong antibacterial resistance to both gram-negative and gram-positive strains, and significant hemostatic ability. The mussel-inspired, catechol-based adhesion mechanism relied on conjugating chemically modified dopamine to a chemically modified gelatin that produced a photocrosslinkable hydrogel platform.

Lastly, cationic polyelectrolyte poly-(diallyldimethylammonium chloride) was incorporated into the polymer matrix to provide a high charge density that exponentially induced antibacterial resistance and hemostatic properties to the resulting hydrogel network.

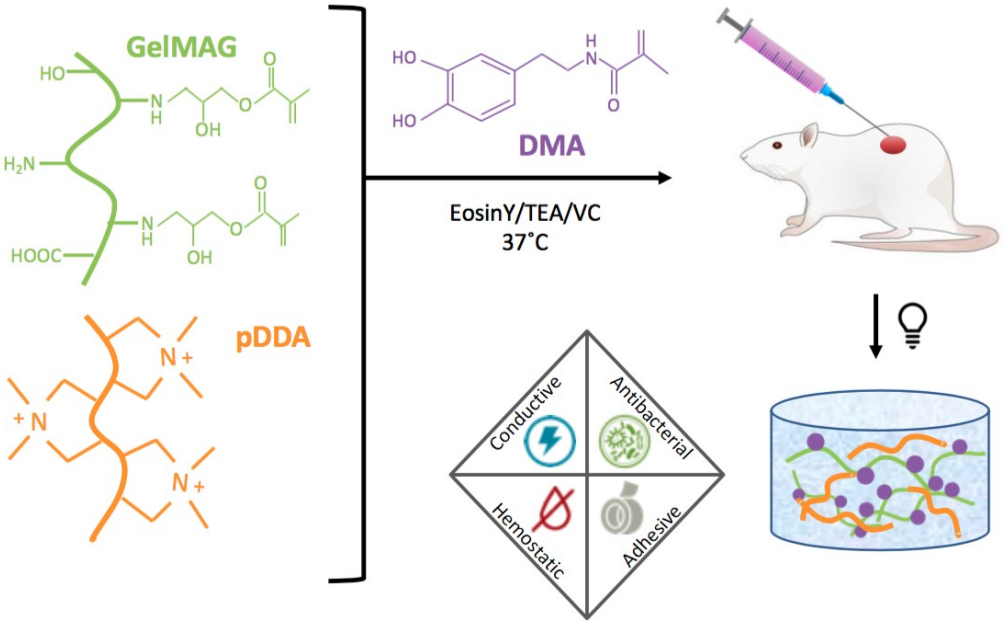

Abstract figure. Chemical schematic and visual representation of the synthesis of a multifunctional hydrogel forwound healing application.

The thesis of Saumya Jain is approved.

Junyoung O. Park

Panagiotis D. Christofides

Nasim Annabi, Committee Chair

University of California, Los Angeles

2022

TABLE OF CONTENTS

LIST OF FIGURES

ACKNOWLEDGEMENTS

Achieving a higher education in a science that will allow me to work in the field of healthcare-directed research has been a lifelong dream of mine. I am incredibly honored and thankful to Dr. Annabi for being my research mentor during my time as a Master's student and supporting my desire to pursue further education in form of a PhD in Chemical Engineering in her lab. I have learned a great deal during the completion of my thesis thanks to my mentor Avijit and my peers in the lab who continuously help me grow. Along with professional relationships, I am immensely grateful for the friendships I have built in the lab. Thank you to Daniel for being a supportive and encouraging friend during our time together in the Annabi lab. I greatly appreciate the collaborative and friendly environment of the UCLA CBE department and eagerly anticipate my future here.

I owe this success to my friends and family, especially, who have always believed in and cheered for me. Thank you to Pam, Abigail, Claire, Kaylene, Dhriti, and Sanika for your endless faith in my abilities and for always helping me push through the difficult moments. And, most of all, thank you to my mom, dad, and sister. From supporting my academic pursuits to making sure I am always happy and healthy, nothing goes uncherished.

CHAPTER I. Introduction

Traumatic injury is one of the leading causes of mortality, accounting for roughly 10% of annual deaths worldwide [1]. Damage to skin tissue or internal organs can be caused by a vast array of incidents, both accidental and violence-related, including motor vehicle accidents, violent crime, falls, burns, etc. For people under the age of twenty-nine years, three of the top five causes of death are injury-induced. Among these instances, 35% of mortality is caused by uncontrollable bleeding at the wound site [2]. Additionally, the rising cases of postpartum hemorrhage sheds light on another leading and preventable cause of material mortality globally [3]. Blood loss in cases of severe physical trauma, childbirth, surgery, and other invasive medical procedures is therefore responsible for a significant percentage of pre-hospital deaths following an injury [4]. Inadequate wound healing in internal or external injuries also creates a heavy financial burden for the healthcare system. In one year in the United States, nonhealing wounds cost up to $50 billion and scars left from traumatic injury or surgical action can cost roughly $12 billion in healthcare [5]. Open or nonhealing acute wounds also present further complications that impede medical treatment. Roughly 10% of all wounds are subjected to bacterial infection, which can exaggerate a patient's immune response (sepsis) to the invading species and lead to tissue damage, organ failure, and mortality [6, 7]. Nosocomial, or hospital-acquired, infections affect 5-10% of all patients, which results in an additional death toll of 75,000 and approximately $30 billion in medical expenditures every year [8]. Thus, it is of utmost importance to maintain hemostasis in all stages of injury and expediate the wound healing process through infection-free and cost-effective means.

Hemostasis, the first step in wound treatment, is the physiological process of stopping blood loss at the site of injury while maintaining adequate circulation of blood and oxygen to

remaining parts of the body to ensure proper organ function. The mechanism of hemostasis acts in two components [9]. Primary hemostasis depends on the activation of platelets to induce aggregation and plug formation while secondary hemostasis refers to the formation of an insoluble fibrin mesh that strengthens the aforementioned platelet plug. There are numerous universally practiced clinical and non-clinical methods with which to alleviate blood loss. Systemic hemostatic agents including blood products, coagulation factors, fibrinogen concentrate, synthetic and allogeneic platelets, etc. have been investigated as potential solutions to copious bleeding [10]. However, systemic administration of a hemostatic agent may take a prolonged amount of time to take effect at the site of injury, which proves to be unsuitable for a sensitive and responsive trauma such as hemorrhage. Additionally, there are limitations concerning the availability, cost, and shelf-life of allogenic solutions such as blood transfusions, dried and frozen plasma, and cryoprecipitate [11-13]. Similar therapies such as fibrinogen concentrate, comprising the final protein in the coagulation cascade, show variable clinical benefit due to the rapid deterioration of fibrinogen which necessitates consistent reapplication to ensure replenishment of the clotting factor in sites of trauma. Dried platelets are another remedy that suffer the drawbacks associated with allogenic products, including poor efficacy, high immunogenicity, unfeasible portability, and risk of bacterial contamination. Synthetic drugs are also used in intravenous therapy for excessive bleeding, especially on the battlefield and in prehospital settings. Tranexamic acid, a systemically administered fibrinolytic inhibitor, proves its potential in treating bleeding by preventing the impairment of blood clots by plasminogen, but it also induces a potential risk of off-target thrombosis and even neuropathy [14, 15]. Systemic coagulopathy can be avoided by localized delivery of a hemostatic agent.

The traditional method for local treatment of hemorrhage involves the mechanical application of pressure to the site of injury with an absorbent material that can also act as a bandage to protect the open wound from the environment. Gauze dressings fit this profile and have therefore predominantly been used throughout the history of hemorrhage treatment in prehospital and combat settings. However, both woven and the prior-developed nonwoven gauze are limited in effectiveness since they risk lint fiber shedding into the injury upon application or removal of gauze as well as adhesion to the wound site, which complicates gauze movement. Additionally, gauze requires consistent replacement to provide a dry environment for blood absorption and to prevent bacterial proliferation. Traditional non-woven gauze has therefore been modified to reduce aforementioned disadvantages. Especially exploited in combat scenarios are material such as zeolites, kaolin, and chitosan that have been investigated to bolster the effects of hemostatic dressings. QuikClot is an example of a heavily used, commercial gauze product that is infused with kaolin, which is responsible for activating coagulation factors that ultimately propagate the formation of a fibrin clot. Incorporation of chitosan in a hemostatic material leads to the emergence of a multifunctional system. The cationic backbone of chitosan prevents coagulopathic bleeding by forming electrostatic interactions with the negatively charged red blood cells. On top of that, chitosan adheres to injured tissue and effectively seals off the site to promote healing. Celox Gauze, HemCon Bandage, and ChitoGauze Pro are examples of commercial gauze that utilize a biomaterial to prevent excessive bleeding [16].

Regardless of these advances, gauze dressings still face limitations in the risk of thromboemboli formation, damage to crucial organs in cases of long-term application, and even the propagation of the progressive phase of shock that is marked by cardiovascular deterioration [17]. Additionally, gauze and other topical hemostatic tools such as sponge, foam, and powder

must be refreshed to ensure hemostatic effect. Removal and reapplication of these agents increase the risk of thromboembolism due to the materials fragile structural state after saturation with blood. Topical hemostatic dressings are also restricted only to surface wounds. Often times when an injury is deep penetrating or originating inside the body, a topical agent will not be able to tend to it. Additionally, when synthetic material is applied within the body, it raises concerns of toxicity of the substance upon local tissue. Synthetic hemostatic dressings used for internal hemorrhage control also require additional surgery for removal of the material since they do not easily biodegrade in a physiologically safe manner. Science thus took inspiration from nature to derive a new species of hemorrhage-combating agents for wound treatment made solely from biomaterial.

The incorporation of nature-derived biomaterial into gauze opened the door to the development of hemostatic agents made only of biologically relevant products. Merging the study of natural substances that would alleviate traumatic bleeding with the design concepts of gauze dressings introduces the use of the hydrogel biomaterial as dressings for wound healing applications. A hydrogel is a three-dimensional (3D) network of hydrophilic polymers that have tunable mechanical and physical properties, allowing mimicking of different tissue systems [18]. Their high water content simulates the native extracellular matrix and their networks provide the mechanical support required for tissue regeneration. Additionally, hydrogels have great potential in the realm of hemostatic agents due to their substantial swelling profile and saturation, which is attributed to the polymer's hydrophilicity and permeability (porosity of the polymer network). Both synthetic and naturally occurring polymers have been used to formulate hydrogels.

Synthetic polymers, including poly(ethylene glycol) (PEG), polycyanoacrylate, and catechol-based polymers, are commonly used to develop hemostatic biomaterials [19]. Commercial PEG-based biomaterials including FocalSeal®, DuraSealTM, and CoSeal®, are

commonly used for hemostasis and wound healing due to their excellent tissue adhesion properties. The interpenetrating polymer network of the PEG hydrogel interacts with chemical moieties on the tissue surface to enable adhesion and tissue sealant behavior. These adhesive biomaterials eliminate the need for sutures or staples to close the wound which can increase the risk of tissue tearing during administration or removal, sepsis, skin reactions, or scarring [20]. In each commercial product, PEG is modified to facilitate use of the hemostatic agent in clinical settings. Chemical modification of PEG allows rapid photopolymerization to a final hydrogel network, which maintains ease of use [21]. However, the use of ultraviolet (UV) radiation utilized to cure the photocrosslinkable biomaterial has deleterious effects on skin such as photodamaging and photocarcinogenesis [22]. Another limitation concerning the photopolymerization of chemically-modified PEG is the production of free radicals that can cause hazardous reactions on tissues [23]. Cyanoacrylate-derived tissue adhesives are another synthetic sealant that form strong covalent bonds both on the surface and within crevices of injured tissues (mechanical interlocking) before rapid polymerization [24]. However, cyanoacrylate glues release toxic byproducts upon degradation that can result in a severe inflammatory response and wound infection [25]. They also lack the mechanical strength to adapt to the treatment of larger abrasions. Due to the overwhelming impediments of synthetic biomaterials, investigation into natural products became favored.

Naturally-derived biomaterials designed from biologically relevant and physiologically safe sources such as polysaccharides and proteins assuage the concerns of cytotoxicity stemming from synthetic-based products [26]. Their advantages include excellent biocompatibility and biodegradability, which eliminates the need for invasive surgical procedures for their removal from an internal site of injury. There is also an abundance of raw materials from which to extract or synthesize the desired bioproduct: a fact that makes the substance more economically accessible.

Hydrogels derived from polysaccharides utilize natural materials such as chitosan, cellulose, dextran, alginate, starch, and hyaluronic acid, among others, to devise a hemostatic agent. As well as its previously mentioned functionalization of gauze products, chitosan has also been used in the realm of naturally-derived hydrogel materials. However, there exist limitations with using chitosan alone as a hemostatic agent. Although the carbohydrate encourages red blood cell coagulation, chitosan is proven to restrict activation of the intrinsic coagulation cascade [27]. Modifications of chitosan can potentially reduce this risk as well as endow the biomaterial with beneficial properties. Chemical functionalization with quaternary ammonium or other highly positively charged moieties can enhance the blood clotting properties already prevalent in the polysaccharide [28]. Cellulose and its derivatives comprise more polysaccharides that are commonly used for wound treatment. Cellulose oxide is known to rapidly absorb expelled fluid, entrap platelets and red blood cells, increase clotting factors, and initiate coagulation. However, cellulose maintains a low pH – due to the large number of carboxyl groups – that makes treatment of sensitive biological systems, such as the nervous or cardiac systems, physiologically unfeasible. Although more sensitive to physiological conditions than their polysaccharide-based counterparts, protein-based hydrogels also contribute to the quest for developing an ideal hemostatic agent.

Protein-based biomaterials offer tunable mechanical strength and intrinsic properties for a wide range of biomedical applications [29]. Naturally occurring structural proteins such as collagen, silk, elastin, and gelatin are commonly used to derive protein-based hydrogels for hemostatic control. Silk fibroin (SF) has excellent hemostatic ability due to its rough surface which accelerates blood coagulation [30]. However, SF-based biomaterial brings concerns of long-term biocompatibility and immune reactions due to the degradation products of SF [29]. Elastin-based proteins have also been investigated for injury treatment since they can be combined with other

polymer systems to enhance adhesion and elastic properties of the resulting tissue sealant or can be chemically modified to produce a photocurable prepolymer [31]. Nevertheless, progress with elastin-based hemostatic agents is hampered by the material's insolubility and structural stability. Gelatin is another versatile protein, derived from collagen, that showcases tissue regeneration potential, but suffers from fast degradation, poor mechanical properties and low shape stability [32].

No singular biomaterial has all the properties required for wound healing. Although some single-component hydrogels retain beneficial properties – chitosan-based hydrogels that impart rapid hemostasis, elastin-based hydrogels that adapt to mobile tissue surfaces, etc. – there is a need for modification or incorporation of multiple polymer systems to develop an ideal therapy for injuries. Many natural polymers have been combined with synthetic agents such as polyacrylamide to mimic the physiological microenvironment of the injured tissue system or to impart beneficial properties to the hydrogel that facilitate wound treatment [33]. However, despite the manufactured benefits, these combinations serve to increase risks of cytotoxicity. There is seldom a biomaterial that harnesses multifunctionality to combat hemorrhage and bacterial proliferation while securing a physiological condition that promotes wound healing at an appropriate time scale.

The current work relies on the functionalization of gelatin to devise a novel, multifunctional hydrogel to be used for hemostatic application. Gelatin is chemically modified with glycidyl methacrylate (GMA) to produce glycidyl methacrylate-modified gelatin (GelMAG). The degree to which GelMAG is methacrylated can be altered in order to control the physical properties of the resulting hydrogel. In order to supply GelMAG with the robust adhesion that is required of tissue sealants, we then take inspiration from the natural phenomena of marine mussel adhesion to surfaces in underwater conditions via catechol chemistry. Catechol-containing

dopamine hydrochloride is chemically modified with methyl methacrylate (MA) to produce dopamine methacrylate (DMA), which is then functionalized onto the GelMAG backbone. The hemostatic and antibacterial mechanism of our hydrogel stems from a third component: poly(diallyldimethylammonium chloride) (pDDA). The polyelectrolyte pDDA is commonly used in antimicrobial agents for its quaternary ammonium-saturated backbone. The heavily cationic polymer promotes electrostatic interactions with negatively charged bacterial cell membranes and effectively disrupts bacterial proliferation [34]. Recent developments with pDDA have incorporated synthetic polymer systems with pDDA to create a biomaterial that can have potential in antibacterial application or cancer therapy. To our knowledge, the polyelectrolyte has largely been underinvestigated for its hemostatic or wound healing potential. We therefore seek to utilize pDDA in our GelMAG/DMA composite hydrogel to attribute antibacterial and hemostatic properties. Our final hydrogel was characterized with mechanical, adhesion, and conductivity testing. *In vitro* antibacterial and hemostatic tests were also performed to assess its ability to prevent infection and control bleeding. Lastly, *in vitro* tests were conducted to prove biocompatibility of the biomaterial using mouse embryonic fibroblast cells. The designed bioadhesive in this study has potential to be used a single material for sealing and repair of internal wounds due to its combined unique properties including hemostasis, antimicrobial, adhesion, and tissue regenerative capabilities.

CHAPTER II. Materials and Methods

2.1 Materials

Gelatin from porcine skin (Gel strength 300, Type A), glycidyl methacrylate (GMA), poly(diallyldimethylammonium chloride) (pDDA), Eosin Y, and triethanolamine (TEA) were all purchased from Sigma Aldrich. Dopamine, N-vinyl-ε-caprolactam (VC), and Dulbecco's phosphate buffered saline (DPBS) were purchased from ThermoFischer Scientific. Methacrylic anhydride (MA) was purchased from Alfa Aesar. Dulbecco's phosphate buffered saline was purchased from Gibco. Nuclear magnetic resonance (NMR) solvents: deuterated dimethyl sulfoxide (DMSO-d6) and deuterium oxide (D_2O) were purchased from Fischer Scientific.

2.2 Preparation of hydrogel

2.2.1 Synthesis of glycidyl methacrylate modified gelatin (GelMAG)

Gelatin was chemically modified with GMA to produce GelMAG through a one-step reaction between gelatin and GMA. First, 10% (w/v) gelatin from porcine skin (Gel strength 300, Type A, Sigma) was dissolved in DPBS at 60˚C while under constant, vigorous stirring to make a gelatin solution. Once fully dissolved, 0.16% (v/v) GMA (Sigma) was added dropwise at 60˚C and under stirred conditions and allowed to react for four hours. The mixture was then diluted (2X) with DPBS to quench the methacrylation. The solution was dialyzed with a 12 to 14 kDa MWCO dialysis tubing for 7 days against deionized water at 50˚C to remove impurities such as salts and unreacted GMA. The clear dialyzed solution was then frozen at -80˚C overnight and then lyophilized for 7 days until a white foam-like solid was produced. GelMAG was stored at 4˚C.

2.2.2 Synthesis of methacrylated dopamine (DMA)

Dopamine was chemically modified with MA to produce DMA using a synthesis that was previously reported to which further modifications were made [35]. Briefly, dopamine hydrochloride at 5% (w/v) was produced in a mixture of borax and sodium bicarbonate solution (5:2) under nitrogenated conditions at room temperature. Subsequently 25% (v/v) of MA tetrahydrofuran solution (0.2 ml/ml) was added to the mixture dropwise. During the reaction, the pH was maintained above 8 by adjustment with sodium hydroxide. The reaction continued overnight until it was washed in triplicate with ethyl acetate. Afterwards, the pH of the aqueous phase was reduced to below 2 by adjustment with hydrochloric acid and the organic layer was separated and concentrated by rotary evaporator and mixed with cool hexane to precipitate DMA. The precipitated DMA was then further purified by using cooled hexane, dried under vacuum conditions, and stored at 4˚C.

2.2.3 Preparation of GelMAG-pDDA hydrogel with and without DMA

Prepolymers without DMA were prepared by mixing 20% (w/v) GelMAG in a photoinitiator solution. The photoinitiator solution was prepared with 0.08% (w/v) Eosin Y, 0.9% (v/v) triethanolamine (TEA), and 0.9% (w/v) N-vinyl-ε-caprolactam. First, VC was mixed in DPBS and allowed to sonicate for one hour until completely dissolved. Then Eosin Y and TEA were added and thoroughly mixed. This light sensitive solution was covered in aluminum foil and stored at 4˚C. GelMAG was then added to Eosin Y/TEA/VC at the aforementioned concentrations and incubating at 37˚C overnight. A light pink, viscous solution was produced when GelMAG was fully dissolved. Next, 0, 0.5, 1, or 2% (v/v) of pDDA was added to the GelMAG solution and quickly mixed (Vortex Genie) to ensure homogenous distribution of the polyelectrolyte. To form

an adhesive hydrogel with DMA, prepolymers containing DMA were prepared by first dissolving 20% (w/v) GelMAG in Eosin Y/TEA/VC at 37˚C overnight, adding 0.1% (w/v) DMA, and then incubating at 37˚C for six hours to allow conjugation of DMA to the GelMAG backbone. The resulting hydrogel appeared orange due to the oxidation of DMA. Finally, 0, 0.5, 1, or 2% (v/v) of pDDA was added to the GelMAG/DMA solution and quickly mixed. The prepolymer solutions either with DMA (G/D/p) or without DMA (G/p) were crosslinked in a polydimethylsiloxane (PDMS) mold for 4 minutes with visible light (450-550 nm) using a LS1000 Focal Seal Xenon Light Source (100 mW/cm^2, Genzyme) to produce crosslinked hydrogels. The hydrogels without DMA appears clear and the hydrogels with DMA appear transparent with a faint yellow-orange tint.

2.3 Chemical and physical characterization

2.3.1 Proton nuclear magnetic resonance (^{1}H NMR) spectroscopy

^{1}H NMR analysis was conducted on the prepolymer solutions and the hydrogels to calculate the degree of chemical functionalization and the degree of crosslinking, respectively. Each type of sample was frozen at -80˚C overnight, lyophilized for two days, and then fully dissolved with a concentration of 10 mg/mL in the NMR solvent at 50˚C. The spectra were obtained in deuterated dimethyl sulfoxide (DMSO-d6) using a 400 MHz Bruker AV400 spectrometer (64 scans). All spectra were processed with phase and baseline corrections and assigned a reference point at the residual singlet peak of DMSO-d6 at 2.54 ppm before analysis. The degree of methacrylation (DM) of GelMAG was defined as the ratio of amine protons on the lysine residues on the GelMAG backbone to free amine protons on the unmodified gelatin backbone. The two vinylic protons residing on the methacryloyl group of GelMAG give rise to two separate singlet peaks at 5.74 and

6.13 ppm. The peak at 2.78 ppm corresponding to the protons on the primary amine in gelatin and the protons on the secondary amine in GelMAG are integrated to determine the DM according to the following equation (Eq. 1).

$$DM\ (\%) = (1 - \frac{I_{2^\circ amine-H\ (GelMAG)}}{I_{1^\circ amine-H\ (gelatin)}}) * 100 \qquad \textbf{Eq. 1}$$

^{1}H NMR analysis was also conducted on dopamine hydrochloride and DMA. Dopamine salt and DMA powder were dissolved at a concentration of 10 mg/mL in DMSO-d6 and the spectra were obtained using a 400 MHz Bruker AV400 spectrometer (64 scans). All spectra were processed with phase and baseline corrections and assigned a reference point at the residual singlet peak of DMSO-d6 at 2.54 ppm before analysis. The methacryloyl protons on DMA give rise to two peaks at 5.33 and 5.64 ppm. ^{1}H NMR analysis was also conducted on GelMAG prepolymer solution and hydrogels with and without both DMA and pDDA to calculate the degree of crosslinking. Both prepolymer solution and hydrogels were prepared, frozen at -80˚C overnight, lyophilized for two days, and suspended in DMSO-d6 solution at 37˚C until fully dissolved. Their spectra were taken with the same spectrometer instrument and processed similarly to previous samples.

2.3.2 Zeta potential

Zeta potential of the hydrogels was determined using a Malvern Zetasizer Nano-Z with the universal DTS1070 folded capillary cells and DTS (Nano) software (version 4.20) at 25˚C to assess the electrical potential of the final biomaterials. Zeta potential measurements were performed for all conditions of prepolymer solution by dissolving them in DI water at a concentration of 50 µg/mL. (N=4)

2.3.3 Scanning Electron Microscopy (SEM)

SEM images were taken of hydrogel samples that were incubated in a bacterial suspension for the antimicrobial test to observe the hydrogel surface after antibacterial testing in order to quantify the bactericidal property of the biomaterial. Sample preparation for SEM required removing the hydrogel from the suspension and washing three times with DPBS. The bacteria were then fixed onto the polymer after 30 minutes of submersion in 2.5% (v/v) glutaraldehyde and 4% (v/v) paraformaldehyde. The samples were again rinsed three times in DPBS and then serially dehydrated in ethanol from 30% to 100%. The hydrogels then underwent critical drying (Tousimis Autosamdri-810 Critical Point Dryer), gold sputtering (Denton Bench Top Turbo-IV Evaporator), and SEM imaging (ZEISS Supra 40VP SEM).

2.3.4 Conductivity

Conductivity of the hydrogel samples was assessed to observe the effect of polyelectrolyte incorporation into the polymer system. PDMS molds held 80 μL of prepolymer solution that was then crosslinked for 4 minutes with visible light. The hydrogels were removed from the mold and quickly dipped in DI water to initiate ionic conductance. The moist hydrogel was placed in between two gold nanochips so that both faces were in contact with the entirety of the sample. Conductivity was measured by connecting the gold chips to a computer with CorrWare® potentiostat software for electrochemical analysis (-0.4 OC to 0.4 OC, 50 mV/S). Taking the slope of the electrical current and voltage data provides conductivity for the measured samples. (N=4)

2.3.5 Mechanical characterization

2.3.5.1 Tensile test

Tensile tests were conducted by pipetting 80 µL of prepolymer solution into a PDMS mold (length: 8 mm, width: 5 mm, height: 1 mm) and then crosslinking for 4 minutes with visible light. The size of the resultant hydrogel was measured using a digital caliper to ensure accurate dimensions. The sample was then placed in between double-sided tensile tape and secured in place by the ends of the gel by using a small amount of super glue. The ends of the tape were clamped to either end of the Instron 5944 mechanical tester to record characteristics and tensile data was collected on Bluehill Universal software. Samples were pulled to failure at a strain rate of 1 mm/min. Ultimate strength was taken at the maximum stress the hydrogel can endure without mechanical failure. Stretchability was taken at the maximum strain the gel can endure before failure. Young's modulus was taken as the slope of the initial linear portion of the stress vs. strain curve at 6 to 10% maximum strain. (N=4)

2.3.5.2. Compression test

Compression tests were conducted by pipetting 80 µL of prepolymer solution into a PDMS mold (diameter: 5 mm, height: 2 mm) and then crosslinked for 4 minutes with visible light. The size of the resultant hydrogel was measured with a digital caliper to ensure accurate cylindrical measurements. The sample was placed in between the compression plates of the Instron 5944 mechanical tester and compressed at a rate of 1 mm/min until mechanical failure. Compression data was recorded using Bluehill Universal software. Compressive modulus was taken as the slope of the linear portion of the stress vs. strain curve at 97 to 99% maximum strain. (N=4)

2.3.5.3 Cyclic compression test

Cyclic compression tests were conducted by pipetting 80 µL of prepolymer solution into a PDMS mold (diameter: 5 mm, height: 2 mm) and then crosslinked for 4 minutes with visible light. After dimensions were confirmed with a digital caliper, the sample was placed in between compression plates of the Instron 5944 mechanical tester (with Bluehill Universal software) and compressed to 50% at a rate of 1 mm/min for 12 cycles. Energy loss was calculated from the last cycle by using the following equation where the loading curve occurs when the sample is compressed, and the unloading curve occurs when the sample is decompressed (Eq. 2). (N=4)

$$Energy\ loss\ (\%) = \frac{area\ under\ loading\ curve - area\ under\ unloading\ curve}{area\ under\ loading\ curve}\ x\ 100 \qquad \textbf{(Eq. 2)}$$

2.3.6 Adhesion characterization

2.3.6.1 Wound closure test

Wound closure tests based on American Society for Testing and Materials (ASTM) test F2458 for wound closure test with some modifications to determine the characterize the biomaterialsadhesive properties. [31] Briefly, the tests were conducted by first ridding all hair and subcutaneous fat from porcine skin tissue. Two pieces of tissue (length: 3 cm, width: 1 cm, height:
0.5 cm) were then secured to glass slides using superglue and then placed together to the ends meet seamlessly. At this junction, 100 µL of prepolymer solution was pipetted in a square (1 cm x 1 cm) to evenly cover both pieces of tissue. The prepolymer was crosslinked for 4 minutes with visible light and then the glass slides were fixed to the clamps of the Instron 5940 mechanical tester where they were pulled apart until hydrogel failure at a rate of 1 mm/min. Adhesion strength data were

collected with Bluehill Universal software at maximum stress and the adhesion energy was taken as the area under the curve of force versus displacement until the maximum displacement. (N=4)

2.3.6.2 Burst pressure test

Burst pressure based on ASTM test F2054 for burst pressure with some modifications was conducted to assess tissue sealant abilities. [31] A custom-built burst pressure device was assembled consisting of a steel base and top holder, syringe pump, pressure sensor, and computer with data collecting software (Pasco Capstone). A piece of dry collagen sheet made of porcine skin was submerged in water and dried thoroughly with a Kimwipe to mimic natural skin. The collagen sheet was secured in the holder while ensuring the sheet is big enough to cover the rubber o ring inside the metal holding device. A puncture (diameter: 1 mm) was made in the center of the collagen sheet and 60 µL of prepolymer solution was pipetted to cover the hole. The hydrogel was formed after 4 minutes of photocrosslinking with visible light. The burst pressure test was then initiated by activating the syringe pump at an air flowrate of 10 mL/min and measuring the pressure at which the hydrogel bursts off the collagen sheet. (N=4)

2.3.7 Antibacterial test

2.3.7.1 Bacteria survival test

The bacterial survival test was conducted by culturing two strains of bacteria: *Pseudomonas aeruginosa* (gram-negative) and *Staphylococcus aureus* (gram-positive). *P. aeruginosa* was cultured by applying the inoculum in the streak plate method (non-overlapping zig zags) onto the surface of Luria-Bertani (LB) agar plates and incubating at 35˚C overnight. S. aureus was cultured by using the streak plate method on Tryptic Soy Agar (TSA) plates and incubating at 35˚C

overnight. The next day, one colony from each strain of bacteria was suspended in their respective growth broths and incubated at 35˚C overnight. Bacterial concentration in the broth was determine by measuring optical density (OD) at 625 nm using the BioTek Eon Microplate Spectrophotometer. Once the OD was between 0.06 and 0.08, the hydrogel samples were added to the bacterial suspension and incubated in 35˚C. On days 1, 3, and 6 of bacterial survival study, optical density of the bacteria and hydrogel suspensions was measured and 100 μL of suspension was evenly spread onto an agar plate (respective to the bacteria strain) and incubated in 35˚C overnight. On days 2, 4, and 7 of the survival study, the colony forming units were counted. (N=3)

2.3.7.2 Zone of inhibition test

The zone of inhibition test was conducted by photocrosslinking 100 μL of precursor solution in a PDMS mold (diameter: 5 mm, height: 2 mm). The resultant cylindrical hydrogels were submerged in DPBS for one hour. Meanwhile, a bacterial suspension with OD 0.06 to 0.08 was spread evenly onto an agar plate respective to the bacterial strain. After one hour of submersion, the hydrogel was removed from the PBS, lightly dried, placed on the surface of the agar plate, and incubated at 35˚C overnight. Zone of inhibition was measured by using a ruler to determine the space between the edge of the hydrogel and the start of the bacteria coverage.

2.3.8 Hemostatic test

The hemostatic test was conducted by activating citrated whole blood (Zen-Bio) with 0.1 M calcium chloride in a 9:1 ratio (blood:$CaCl_2$). Before activating the blood, equal amounts of precursor solution that had been treated with visible light to form a hydrogel was prewarmed for 5 min. The activated blood mixture was vigorously stirred for 5 seconds and then added to the well

plates. At specific time points, the blood clotting was quenched with saline solution and nonclotted liquid was removed to determine how much blood formed a clot. At the same time as qualitative assessment of clotting behavior at each predetermined time point, a quantitative assay was conducted on the nonclotted liquid that was removed from the well plate. One drop (2µL) of the liquid was dispensed into the Nanodrop™ One/One^{C} Microvolume UV-Vis Spectrophotometer (ThermoFischer) to measure the absorbance of hemoglobin at 540 nm. A baseline correction at 750 nm was included for the entire spectrum. An absorbance profile depicted the amount of hemoglobin in the nonclotted blood throughout duration of the hemostatic test. The blood clotting index (BCI) was determined at 35 minutes (when the sample with fastest clotting effect was fully clotted) using the following equation (Eq. 3) where A is the absorbance at 540 nm. (N=4)

$$BCI = \frac{A_{sample}}{A_{whole\ blood\ control}} x\ 100 \quad \textbf{(Eq. 3)}$$

Lastly, the clotting weight was measured by quenching blood clotting at 40 min (when the sample with fastest clotting effect was fully clotted) and determining the mass of the clot formed by each sample. (N=4)

2.3.9 Swelling ratio measurement

Swelling profile for all samples was obtained by photocuring the prepolymer into a hydrogel and then incubating in DPBS at 37˚C for 48 hours. The dry mass (W_o) was reported immediately after sample preparation, and the mass taken at predetermined time points (W_i) was measured after blot-drying the incubated samples. Swelling ratio was determined using the using the following equation (Eq. 4). (N=4)

$$Swelling\ ratio\ (\%) = \frac{W_i - W_o}{W_o}\ x\ 100 \quad \textbf{(Eq. 4)}$$

2.3.10 Degradation rate

Degradation profile for all samples was obtained by first photocuring the prepolymer into a hydrogel as explained before. The samples were fully submerged in 2 U/mL solution of collagenase type II and then incubated at 37˚C for 4 weeks. The collagenase solution was refreshed every 2-3 days in order to maintain constant degradation activity. The dry mass (W_o) was recorded immediately after sample preparation and the wet mass (W_i) was measured at predetermined time points after blot drying the submerged sample in order to calculate the degradation ratio of the hydrogel according to the following equation (Eq. 5). The degradation ratio was then normalized. (N=4)

$$Degradation\ rate\ (\%) = \frac{W_o - W_i}{W_o}\ x\ 100 \quad \textbf{(Eq. 5)}$$

2.3.11 *In vitro* biocompatibility studies

Cellular biocompatibility studies were conducted on mouse embryonic lung fibroblast cells (3T3-Swiss albino cell line, ATCC). Cells were cultured in Dulbecco's Modified Eagle's Medium (DMEM, ATCC) that contains 4 mM L-glutamine, 4500 mg/L glucose, 1 mM sodium pyruvate, and 1500 mg/L sodium bicarbonate. DMEM was treated with 10% fetal bovine serum (FBS) and 1% penicillin/streptomycin antibiotics prior to use. Fibroblast cells were cultured on a Falcon® polystyrene tissue culture flask with a vented cap (Corning) and incubated at 37˚C with 5% CO_2 infusion until use. Hydrogel condition GelMAG/DMA/2% pDDA was assessed for the cell study, with GelMAG and no hydrogel conditions used as a control. Hydrogels were prepared using

previously stated methods and loaded into a transwell insert within a 24-well plate. Fibroblast cells were then seeded onto the 24-well plate at a concentration of 1 x 10^4 cells/mL and both cells and transwell insert were covered entirely with DMEM.

2.3.11.1 Live/Dead cytotoxicity assay

A live/dead viability assay was conducted on the fibroblast cells using GelMAG and GelMAG/DMA/2% pDDA to determine cell viability. The assay solution was first prepared by making a solution with 0.05% Calcein-AM and 0.2% ethidium homodimer-1 in DPBS without light conditions. Culture media was removed from cell-containing wells and replaced with 300 µL dye solution to cover the entire bottom of the well. The well plate was covered with aluminum foil and incubated in 37˚C for 30 minutes. The dye solution was then removed, replaced with DPBS, and the plate was imaged with the AxioObserver Z1 inverted microscope (Zeiss). Live cells appeared green and apoptotic cells appeared red. Cell viability was determined by dividing the number of live cells by the total cell count. (N=3)

2.3.11.2 Actin/DAPI staining

Actin/DAPI staining was conducted on the fibroblast cells exposed to GelMAG and GelMAG/DMA/2% pDDA to assess cell morphology and spreading. The fibroblast cells were first fixed with a wash with 4% (v/v) paraformaldehyde (10 min, room temp) and a subsequent wash with DPBS upon removal of the paraformaldehyde. Next, cells were washed with 0.5% (v/v) Triton-X (10 min, room temp). When Triton-X was removed, the cells were washed three times with DPBS (5 min per wash). Finally, 1% (v/v) BSA was added to the cells (30 min, room temp). Once the cells were fixed, a staining mixture of 0.1% (v/v) Phallodin and 0.05% (v/v) DAPI in

DPBS was used to cover the entire bottom of the cell-containing well (10 min). Wells were washed three times with DPBS (5 min per wash) and then imaged with the AxioObserver Z1 inverted microscope (Zeiss). Actin filaments were stained green and nuclei were stained blue. Cell spreading was quantified by determining the positively stained F-actin per unit area. (N=3)

2.3.11.3 PrestoBlue™ metabolic activity assay

A PrestoBlue™ assay was conducted on the fibroblast cells using GelMAG and GelMAG/DMA/2% pDDA 2% to assess cell metabolic activity based on the procedures provided by the manufacturer. Cells were ridden of DMEM and treated with a 10% (v/v) solution of PrestoBlue in DMEM in dark conditions. The well plate was covered in aluminum foil and incubated in 37˚C for 45 minutes. After the incubation period, 100 µL of PrestoBlue™ reagent from each well was placed into a 96-well plate where the absorbance was measured at 600 nm using Gen5 3.04 Microplate Reader and Imaging Software and Synergy LX Multi-mode Reader. The cell-containing wells were then devoid of PrestoBlue™ reagent, washed three times with PBS, and supplemented with DMEM. (N=3)

2.3.12 Statistical analysis

Results were presented as mean ± standard deviation (SD) (*$P < 0.05$, **$P < 0.01$, ***$P < 0.001$, ****$P < 0.0001$). One-way or two-way analysis of variance (ANOVA) t-tests were performed followed by Tukey's test for statistical analysis (GraphPad Prism Version 8.4.3).

CHAPTER III. Results and Discussion

3.1 Formulation of GelMAG hydrogel

GelMAG was synthesized by directly reacting gelatin and GMA in PBS at 50˚C (Fig. 1A). Since the reaction occurs in a slightly basic condition, the amine and hydroxyl functional groups on the lysine residues of gelatin react with the less sterically hindered carbon on the epoxide region of GMA. ^{1}H NMR spectroscopic analysis was performed to determine the success of GMA attachment (Fig. 1B, Supporting Fig. 1). The emergence of two peaks at 5.74 and 6.13 ppm correspond to the two vinylic protons of the methacryloyl group. Additionally, monitoring the lysine peak at 2.78 ppm depicted how many amine groups have been substituted with methacryloyl groups. Decreased integration of the lysine peak proved a successful reaction between gelatin and GMA. The degree of methacrylation was calculated with ^{1}H NMR data to be approximately 50% based on the consumption of lysine peaks (Eq. 1). DMA was synthesized by reacting dopamine hydrochloride and MA in a borax and sodium bicarbonate mixture. ^{1}H NMR analysis proved successful methacrylation of dopamine hydrochloride due to the emergence of two peaks at 5.33 and 5.64 ppm, corresponding to the protons on the methacryloyl carbon (Fig.1B, Supporting Fig 2).

The synthesized GelMAG (20% w/v) and DMA (0.1% w/v) were mixed in a photoinitiator solution containing 0.08% (w/v) Eosin Y, 0.9% (v/v) TEA, and 0.9% (w/v) VC to form a hydrogel after photocuring with visible light for four min (Fig. 1C). Another photoinitiator, lithium phenyl-2,4,6-trimethylbenzoylphosphinate (LAP) at 0.05% (w/v) was initially investigated alongside Eosin Y/TEA/VC, but the latter was preferred since it produced a more mechanically durable hydrogel when crosslinked with a visible light source (LS1000 Focal Seal) that operated at 450-

550 nm (Supporting Fig. 3). Once Eosin Y/TEA/VC was selected as the photoinitiator, the ratio of each component was optimized.

Eosin Y is a Food and Drug Administration (FDA)-approved photoinitiator that is excited by visible light (450-550 nm) and has previously been used in the production of the photocrosslinkable lung sealant FocalSeal® [36]. After light excitation of Eosin Y from the ground state into a triplet state, Eosin Y deprotonates the co-initiator TEA. The remaining TEA radical then initiates radical formation on the electrophilic methacryloyl group on GelMAG, which interacts with other methacryloyl groups to form a crosslinked polymer. VC is a co-monomer that is used to generate enough radicals to accelerate the polymerization reaction.

Further testing was conducted with GelMAG hydrogels made using different concentrations of Eosin Y/TEA/VC in order to assess which concentration of each component of the photoinitiator solution gave desired mechanical properties (Supporting Fig. 4). Out of the concentrations of photoinitiator solution used to prepare the GelMAG/2% pDDA hydrogels, the 0.08% (w/v) EosinY, 0.9% (v/v) TEA, and 0.9% (w/v) VC curated the biomaterial with highest ultimate strength and Youngs modulus at 90 ± 9 kPa and 196 ± 29 kPa, respectively. This proved to be notably higher than the same hydrogel prepared with 0.16% (w/v) EosinY, 1.8% (v/v) TEA, and 1.8% (w/v) VC which gave lower ultimate strength and Youngs modulus at 70 ± 5 kPa and 80 ± 29 kPa, respectively.

To form the hydrogel, GelMAG was dissolved in 0.08% (w/v) EosinY, 0.9% (v/v) TEA, and 0.9% (w/v) VC. Next, DMA was added and rapidly mixed in order to prevent coacervation of the polymer due to the saturated negative charge in DMA. DMA was allowed to conjugate onto the GelMAG backbone for 6 hours 50˚C until the solution took an orange/brown color. After DMA

was conjugated, different concentrations of pDDA were added and rapidly mixed to prevent aggregation, caused by the high charge density of the polyelectrolyte.

Prepolymer and crosslinked biomaterials underwent ^{1}H NMR spectroscopic analysis to prove the formation of a dual polymer network and catechol functionalization as well as to monitor the degree of crosslinking (Fig. 1E). The aromatic peaks of DMA reside at 7.44 ppm (highlighted purple), next to the aromatic peaks of Eosin Y at 7.36 ppm. We see the aromatic peaks of DMA persist after crosslinking of the prepolymer solution while those of Eosin Y largely diminish. Incorporation of DMA into the GelMAG prepolymer solution also results in a broadening of the peak at 8.1 ppm due to the overwhelming amount of catechol alcohol groups. The methyl protons adjacent to the quaternary ammonium of pDDA reside at 2.97 ppm (highlighted orange), which do not exist in the biomaterial lacking pDDA. GelMAG was also confirmed by analyzing the methacryloyl protons, residing at 5.70 and 6.08 ppm, of the prepolymer and crosslinked material highlighted green). GelMAG that was crosslinked to produce the GelMAG hydrogel observe a complete erasure of the methacryloyl proton peaks, indicating 100% crosslinking (Eq. 1). The GelMAG/DMA solution was not fully crosslinked, as seen by the minimal peak emittance in the GelMAG/DMA hydrogel, likely due to DMA blocking the methacrylate residues on GelMAG from crosslinking with other GelMAG strands. The GelMAG/DMA hydrogel exhibited 40% crosslinking, confirmed by ^{1}H NMR analysis of the methacryloyl proton consumption (Eq. 1, Supporting Fig. 5). The addition of pDDA to GelMAG also served to decrease the degree of crosslinking to 60% (Supporting Fig. 5). However, the incorporation of both DMA and pDDA to GelMAG resulted in an increase in crosslinking density to 77% most likely due to the interactions between DMA and pDDA which free the methacryloyl residues for GelMAG-GelMAG crosslinking (Supporting Fig. 5).

The final prepolymer solutions were thermosensitive and therefore underwent gelation at room temperature and turned back into viscous solutions at 37˚C (Fig. 1D). The chemical interactions that occurred to form the hydrogel matrix included covalent interactions between methacryloyl groups on GelMAG or between methacryloyl groups on GelMAG and DMA (Fig. 1C) [37]. Hydrogen bonding also occurred between amine, hydroxyl, and carboxyl functional groups on GelMAG, between the catechol groups of DMA, or between GelMAG and DMA. In addition, π-π stacking occurred between the adjacent phenyl rings of DMA. Electrostatic interactions also occurred between the pendant quaternary ammonium groups on pDDA and nucleophilic functional groups on GelMAG.

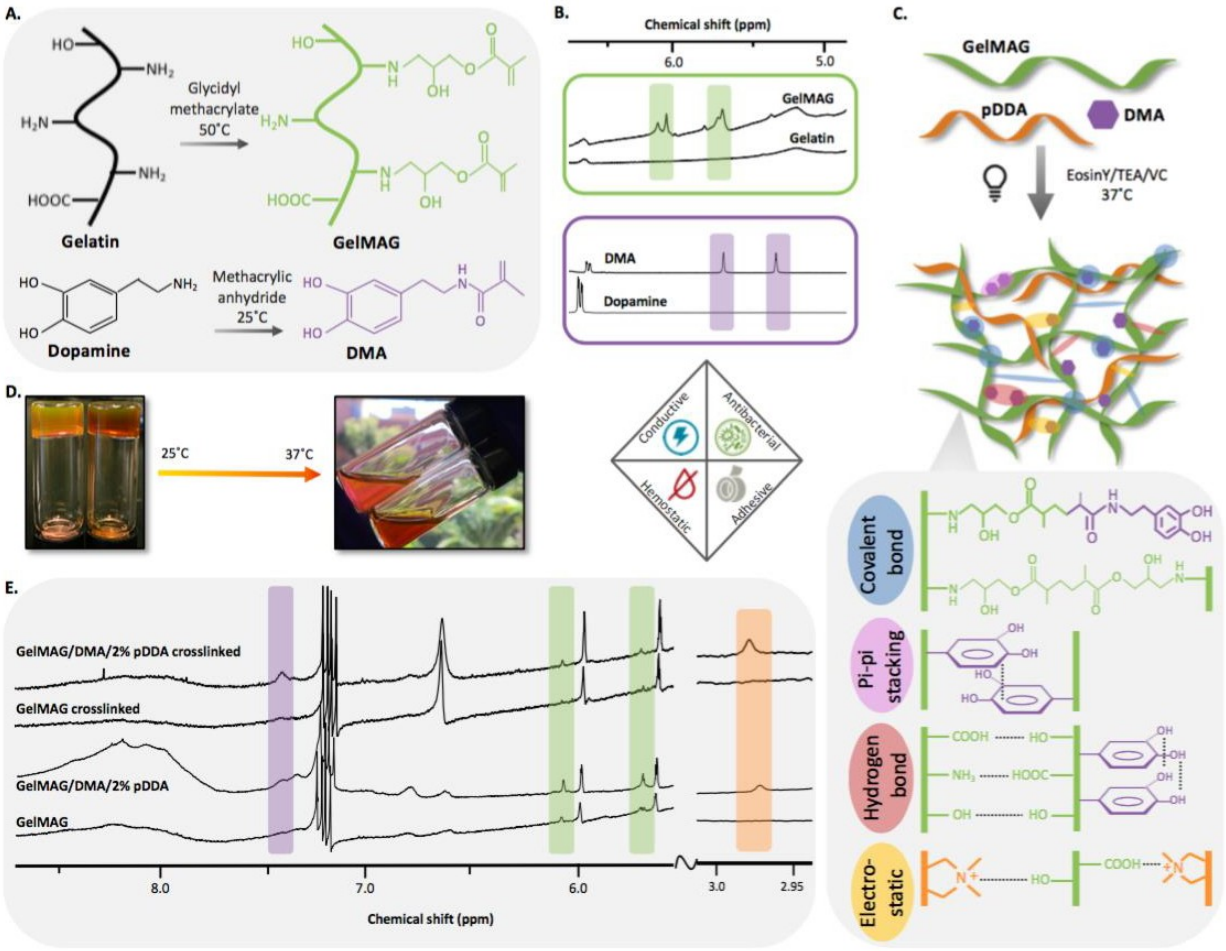

Figure 1. Synthesis and characterization of G/D/p hydrogel. **(A)** Chemical synthesis to procure GelMAG from gelatin and DMA from dopamine. **(B)** ^{1}H NMR for each synthesized product in part (A). **(C)** A visual representation of the hydrogel formation wherein mixing GelMAG, DMA, and pDDA with EosinY/TEA/VC and treating with visible light achieves a three-dimensional polymer network with illustrated chemical interactions. **(D)** Visual representation of thermosensitive prepolymer solution of GelMAG and GelMAG/DMA. **(E)** ^{1}H NMR of the prepolymer and crosslinked solutions of GelMAG with and without DMA and/or 2% pDDA.

3.2 Physical characterization of GelMAG/DMA/pDDA hydrogel

Wound healing applications require a mechanically robust material that can withstand the mobility of elastic tissue such as skin and internal organs. Although numerous biomaterials have been developed for the sealing and healing of injured elastic organs, very few possess the stretchability and mechanical tunability to mimic the wound site [38]. Even commonly used sealants like fibrin-based Tisseel, PEG-based CoSeal, and cyanoacrylate-based Dermabond retain low tensile properties (under 10 kPa and 15% stretchability) that ensure mechanical failure when used on an elastic biological surface [39]. In order to assess the mechanical properties of the GelMAG hydrogel with and without DMA and varying concentrations of pDDA (0.5%, 1%, and 2% (v/v)), all biomaterial compositions underwent tensile and compression testing (Fig. 2). Tensile testing was used to characterize the ultimate strength, stretchability, Youngs modulus, and toughness of the hydrogels (Fig. 2A). The photocured biomaterials were secured to an Instron apparatus and stretched until mechanical failure (Fig. 2A v). The pure 20% (w/v) GelMAG hydrogel had an ultimate strength of 139 ± 13 kPa which decreased to 88 ± 12 kPa after adding 0.5% pDDA (Fig. 2A i). Incorporation of the polyelectrolyte into the pure GelMAG hydrogel decreases hydrogen

bonding interactions between the amine, hydroxyl, and carboxyl moieties on the GelMAG backbone since these functional groups engaged in electrostatic interactions with the pendant quaternary ammonium groups on pDDA, as well as decreases the degree of crosslinking, as previously discussed. When the concentration of pDDA was increased, this effect was overcome likely due to the substantial amount of electrostatic interactions that were initiated by the cation-saturated polymer. Therefore, the GelMAG hydrogel containing 2% pDDA has no statistical difference in strength from pure GelMAG, indicating that mechanical strength was not compromised in the formulation of the resulting biomaterial.

We also studied the effect of DMA addition on mechanical properties. It was found that after the addition of DMA into the pure GelMAG system, there was a decrease in ultimate strength at 102 ± 7 kPa from that of the pure GelMAG hydrogel. DMA causes this mechanical weakening by covalently interacting with the methacryloyl residues on the GelMAG backbone and therefore consuming the reactive moieties that affect the degree of crosslinking of the formulated hydrogel [37]. The polymer network was not as tightly connected, allowing for deformation at lower tensile stress compared to pure GelMAG. When pDDA was added to the GelMAG/DMA hydrogel, we observed a similar decrease in ultimate strength at lower concentrations of pDDA and a return to original hydrogel strength upon addition of higher concentrations of pDDA, likely due to a substantial amount of cation-π interactions between pDDA and DMA. When 2% pDDA was added into GelMAG/DMA, there is no significant difference in its strength (100 ± 8 kPa) compared to GelMAG/DMA, again due to the significant amount of electrostatic interactions that occur with the polyelectrolyte.

The stretchability of the GelMAG hydrogel was not statistically affected by the incorporation of varying concentrations of pDDA (Fig. 2A ii). However, the slight rise in

stretchability from GelMAG hydrogel at 83 ± 7% to the GelMAG/2% pDDA hydrogel at 91 ± 15% can be attributed to the abundance of quaternary ammonium groups on pDDA and nucleophilic functionalities on GelMAG that encouraged the reformation of the electrostatic interactions when the hydrogel was undergoing strain. After conjugation of DMA into theGelMAG hydrogel, there was a significant rise in stretchability at 201 ± 8% which can be attributedto the longer polymer side chain that formed when DMA covalently attached to the methacryloylgroup on GelMAG. The longer sidechain assisted in steric blocking of methacryloyl groups and effectively decreased the crosslinking density of the hydrogel, which resulted in a softer and more elastic material (Fig. 1E). Adding pDDA to the GelMAG/DMA hydrogel may have also compromised crosslinking density due to steric blocking of methacryloyl groups while increasing the amount of electrostatic interactions that resulted in higher material stretchability (Supplementary Fig. 5). This explains the increase in stretchability observed in the GelMAG/DMA hydrogel when pDDA is increased from 0.5% (166 ± 14% stretchable) to 2% (208 ± 15% stretchable).

The Youngs modulus of GelMAG hydrogels with ranging concentrations of pDDA were statistically similar, but the addition of DMA resulted in a drop from 176 ± 10 kPa to 79 ± 5 kPa (Fig. 2A iii). The higher elasticity of the hydrogels containing both DMA and 2% pDDA resulted in a lower Youngs modulus at 36 ± 2 kPa. Material toughness remained consistent in all compositions but increased in the GelMAG/DMA hydrogel with higher pDDA concentration since these fabrications contained more physical interactions between unconjugated polymers and fewer chemical interactions that result in more brittle products (Fig. 2A iv).

Hydrogel samples underwent compression testing to further characterize mechanical properties (Fig. 2B). Cylindrical samples were placed in between steel plates and compressed till

mechanical failure (Fig. 2B iii). The initial addition of 0.5% pDDA to the GelMAG hydrogel decreased compression modulus from 60 ± 5 kPa to 40 ± 6 kPa due to the decreasing crosslinking density that cannot withstand compressive strain (Fig. 2B i). At higher pDDA concentrations, crosslinking density is decreased the therefore so is the compression modulus. When pDDA is added to the GelMAG/DMA hydrogel, this phenomenon causes a further decrease in compression modulus from 71 ± 7 kPa to 47 ± 8 kPa. Cyclic compression successfully monitored compressive energy loss after twelve cycles of compression (Fig. 2B ii). There is no notable change in energy loss among all hydrogel compositions, but mechanical softening upon incorporation of DMA and pDDA results in a slight increase in energy loss from 14 ± 2 kPa (GelMAG) to 25 ± 3 kPa (GelMAG/DMA/2% pDDA).

The retention of notable elasticity in a material with high mechanical strength provides benefits for use in the realm of tissue engineering. Aside from surpassing the mechanical properties of commercial tissue sealants which fail to mimic either the strength or elasticity of native tissue, our hydrogel is comparable or enhanced in physical ability when compared to recently developed gelatin-based biomaterials. For example, in our previous work, we engineered a surgical sealant based on chemically modified gelatin with optimized formulation to bolster tissue adhesion. The methacryloyl-modified gelatin, or GelMA, was found to achieve a notable tensile strength of roughly 50 kPa at higher GelMA concentrations (25% (w/v)) but at compromised elasticity (< 10%). [40] In another work, we developed a methacryloyl and catechol modified gelatin, or GelMAC, to adhere to tissue, but although this work provided higher adhesion at about 40 kPa, it suffered from lower mechanical properties due to the stiffness of the UV-crosslinked material [41]. Other biomedical advances utilize gelatin and dopamine to produce a bioadhesive, but even after optimizing degree of dopamine conjugation to gelatin, the resulting hydrogel retains low adhesion

under 20 kPa [42]. In conclusion, our biomaterial possesses notable strength without compromising elasticity and adhesion ability, a fact that enhances its potential for wound treatment.

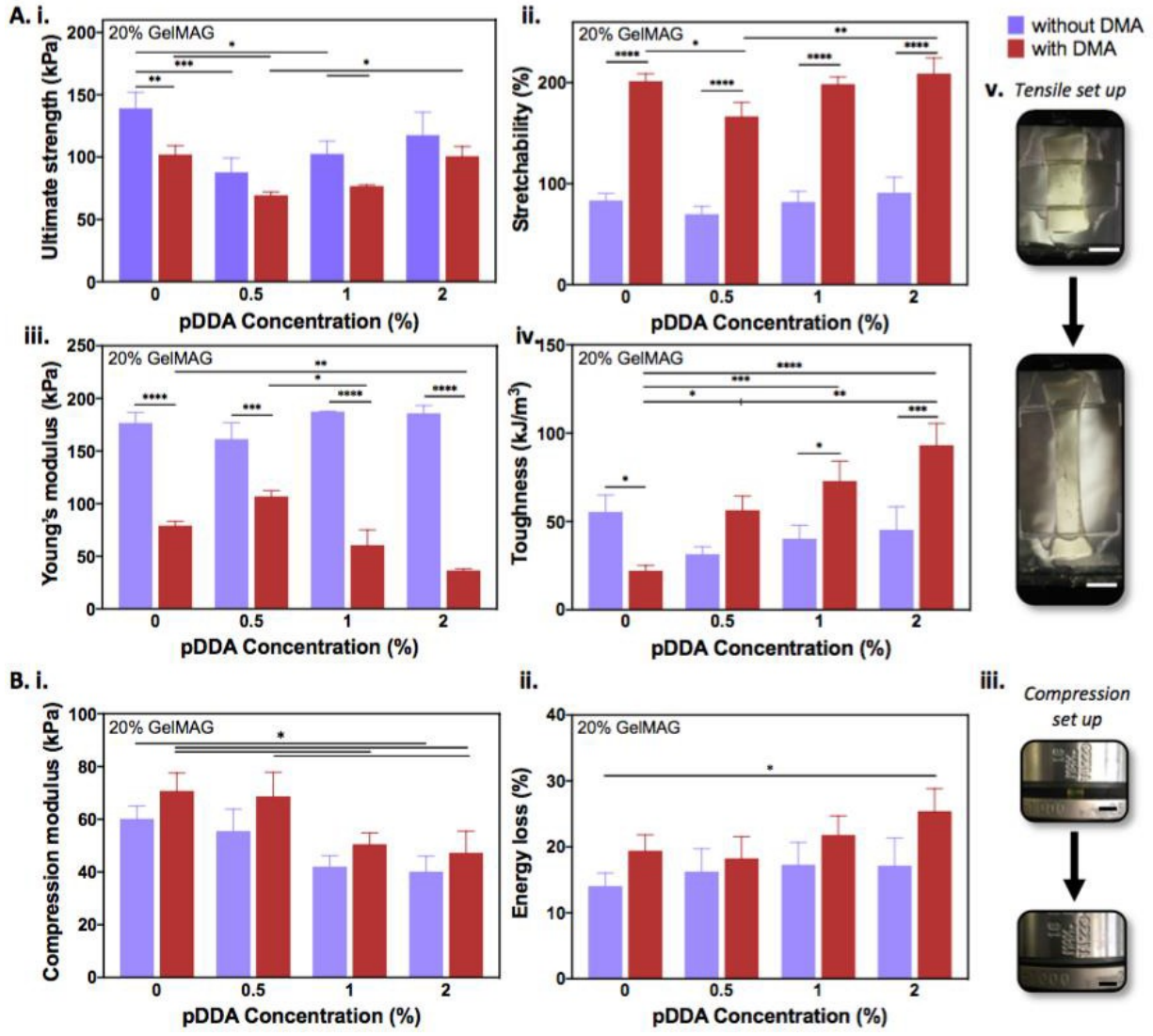

Figure 2. Mechanical characterization of G/D/p hydrogel. (A) Tensile tests on GelMAG hydrogel with and without DMA and varying concentrations of pDDA quantified **(i.)** ultimate strength, **(ii.)** stretchability, **(iii.)** Youngs modulus, and **(iv.)** toughness. **(B)** Compression tests on all hydrogel conditions quantified **(i.)** compression modulus and **(ii.)** energy loss during 12th cycle

of the cyclic compression test. Data are represented as mean ± SD (*P < 0.1, **P < 0.01, ***P < 0.001, ****P < 0.0001, N=4). Scale bar: 5 mm.

3.3 Measurement of adhesive properties of GelMAG/DMA/pDDA hydrogel

Along with mechanical tunability, pivotal is quality of durable adhesion in a biomaterial for wound healing application. Many commercial products lack adhesive properties upon biological surfaces, especially in cases of wet conditions as are present in injuries where blood surrounds the wound site. Human plasma-based Eviseal®, PEG-based Coseal™, and fibrin-based Tisseel™ possess an adhesion strength less than roughly 25 kPa, which increases chances of material detachment from the injured region before sufficient tissue repair [43-44]. Therefore, adhesion testing using two models of assessment (ASTM F2458 and F2054) were conducted to thoroughly quantify the adhesive property of the hydrogel samples (Fig. 3). The porcine skin model was used to quantify adhesive strength and energy through a wound closure experiment (Fig. 3A). The GelMAG hydrogel has an adhesion strength of 25 ± 1 kPa which remained constant as pDDA was added (Fig. 3A i). A significant amount of current research in bioadhesives sustains inspiration from mussels, geckos, and sandworms for their natural mechanisms of powerful adhesion to underwater or wet surfaces [45]. Likewise, our hydrogel mobilizes mussel-inspired adhesion techniques to create an ideal candidate for tissue repair under exsanguination conditions. Dopamine is a derivative the amino acid l-3,4-dihydroxyphenylaniline (L-DOPA) that is prevalent in the marine blue mussel *Mytilus edulis* that is widely studied for its robust adhesion to chemically diverse surfaces in aqueous environments [46]. The oxidized and unoxidized forms of L-DOPA participate in covalent or coordinate bond interactions with organic and inorganic surfaces, respectively, in wet conditions. Further hydrogen bonding interactions from catechol-alcohol groups and Michael addition reactions stemming from the aromatic region of dopamine derivatives result in robust

adhesion to biological surfaces (Fig. 3A iii). After incorporation of this durable anchoring system in the form of DMA to the GelMAG hydrogel, the adhesion strength was enhanced to 40 ± 3 kPa. Upon addition of higher concentrations of pDDA to the GelMAG/DMA hydrogel, we observed an initial decrease and subsequent increase in adhesion strength. Among dopamine derivatives like polydopamine, cation-π interactions take precedence over π-π or covalent interactions when assessing the cause of the polymer adhesion strength. Previous reports of density functional theory (DFT) simulations which monitor adsorption of dopamine derivatives on cationic layers confirmed that the high π-conjugated electron density of DMA enables strong cation-π interactions in an aqueous environment (Fig. 3A iii) [47]. Therefore, within the GelMAG/DMA/0.5% pDDA hydrogel, the cationic polymer engages with DMA through opposite dipole orientations and reduces DMA interaction with the biological surface, represented by a decreased adhesion strength of 30 ± 2 kPa. However, adding higher concentrations of pDDA unsheathes the synergistic relationship between cation-π interactions and hydrogen bonding interactions in aqueous environments, which is theorized to be responsible for mussel-inspired wet adhesion [48]. The polyelectrolyte also engages in electrostatic interactions with functional moieties on the tissue surfaces, which promotes overall adhesion ability. Therefore, as pDDA concentration was increased in the GelMAG/DMA hydrogel, adhesion strength was also increased to 45 ± 1 kPa. The adhesion strength of all tested biomaterial vastly outperforms commercial surgical sealantsCoseal® and Progel™. Both Coseal® and Progel™ are FDA-approved polyethylene glycol (PEG)-based material where Coseal is used as a hemostatic tissue adhesive with an adhesive strength of 2 ± 0.5 kPa and Progel is used as an air leak sealant with an adhesive strength of 1.3 ± 1 kPa.

The stiffer mechanical properties of GelMAG hydrogels with varying pDDA levels, characterized by lower stretchability and higher Youngs modulus (Fig. 2A ii-iii), impacted the

adhesion energy when tested on porcine tissue (Fig. 3A ii). The higher stiffness and lower failure strain translated directly to a lower adhesion energy, at 10 ± 2 kPa, with no statistical difference upon increase of pDDA concentration [49]. On the contrary, the GelMAG/DMA hydrogel, with its higher elasticity and lower modulus, profiled a softer biomaterial with a higher adhesion energy until adhesive failure at 43 ± 5 kPa. The higher adhesion energy was attained through energy dissipation within the material through plastic deformation [50]. As pDDA was added to the GelMAG/DMA system, there was a further enhancement in failure strain and material softness, which resulted in a decreased adhesion energy, averaging 26 ± 1 kPa for all pDDA conditions. This was still an improvement from commercial sealants Coseal®, which has an adhesion energy of 1.6 ± 0.2 kPa, and Progel™, which has an adhesion energy of 0.9 ± 0.5 kPa.

Burst pressure testing was also conducted using a custom-built burst pressure setup to further assess adhesion characteristics of the biomaterials (Fig. 3B). An air pump guided a syringe to continuously administer air to an entrapped, punctured collagen sheet that was secured between air-tight steel plates, in order to assess the pressure (digitally monitored) at which the sealant can withstand on a punctured collagen sheet (Fig. 3B i). Burst pressure adhesion trends followed a similar trend to the adhesion strength for all hydrogel systems. The GelMAG hydrogel sustained a burst pressure of 31 ± 3 kPa for all pDDA concentrations (Fig. 3B ii). GelMAG/DMA exhibited enhanced adhesion at 38 ± 2 kPa due to catechol-based interactions with biological surfaces. Adding pDDA further enhanced the pressure that the hydrogel could withstand before adhesive failure to 51 ± 5 kPa, which is attributed to the cation-π and hydrogen bonding interactions between pDDA, DMA, and tissue surfaces.

The range of adhesive strength possessed by our material surpasses that of recent literature inspired by catechol adhesion mechanisms. Reports have used a polydopamine and

polyacrylamide dual network achieved a highly stretchable biomaterial at about 2500% extensibility [51]. However, the material lacked the tensile strength (~ 10 kPa) and adhesion strength (5-17 kPa) to effectively heal injured tissue on motive organs such as skin and lungs. Additionally, the biomaterial presented risk of cellular toxicity due to inclusion of the synthetically derived polyacrylamide. Meanwhile, natural polymers like hyaluronic acid have been functionalized with dopamine for multiscale bioadhesion but possess low adhesion strengths of around 10 kPa [52]. Therefore, regardless of biocompatibility, the hydrogel does not constitute an ideal candidate for tissue sealing. Our previously described work employing dopamine functionalization to chemically modified gelatin (GelMAC) depicted a notable adhesion strength of around 45 kPa but lacked in the extensibility necessary to adapt to dynamic surfaces [41]. Gelatin has also been reported to be conjugated with dopamine and combined with graphene oxide to impart a hemostatic property to the resulting sealant [53]. After optimizing the concentration of graphene oxide (GO), the material was shown to reduce blood loss by 70% in a rat hepatic hemorrhage model, but the tensile and adhesion strengths are relatively low (both under 20 kPa) and the GO particles pose a risk of cytotoxicity. On the contrary, our GelMAG/DMA/pDDA hydrogel showcases exemplary adhesion ability, far exceeding commercial and recently developed tissue sealants, without sacrificing other essential properties like tensile strength and elasticity, all of which characterizes an effective agent for tissue healing.

The conductive properties of the hydrogel samples were also analyzed to attribute a cause for future developments of multifunctionality (Fig. 3C). The GelMAG hydrogel exhibited an ionic conductivity of 0.11 ± 0.02 S/m. When pDDA concentrations increased in the GelMAG hydrogel, so did the cationic charge density, which explains the rise in conductivity to 0.30 ± 0.03 S/m for the GelMAG/2% pDDA biomaterial. When DMA was introduced to the GelMAG hydrogel,

conductivity was significantly enhanced to 0.43 ± 0.07 S/m. Through zeta potential analysis, it was observed that DMA conjugated to GelMAG has a more negative potential than the GelMAG hydrogel without DMA (Supporting Fig. 6). Since DMA carries negative charge, it is thought to act as a "doping" agent to magnify the conductive properties of the pDDA-containing samples [59]. Increasing pDDA concentration in GelMAG/DMA hydrogels further bolstered their conductive property to 0.78 ± 0.14 S/m for 1% pDDA. The insignificant decrease in conductivity in the GelMAG/DMA/2% pDDA hydrogel can be attributed to a saturation of DMA-induced doping and subsequent quenching of pDDA cations with the negative charge of DMA. Our designed hydrogel falls in the range of conductivity possessed by native cardiac and nerve tissue and surpasses the conductivity of previously developed carbon-based, polymer-based, and ionic liquid-based biomaterial (Fig. 3C iii).

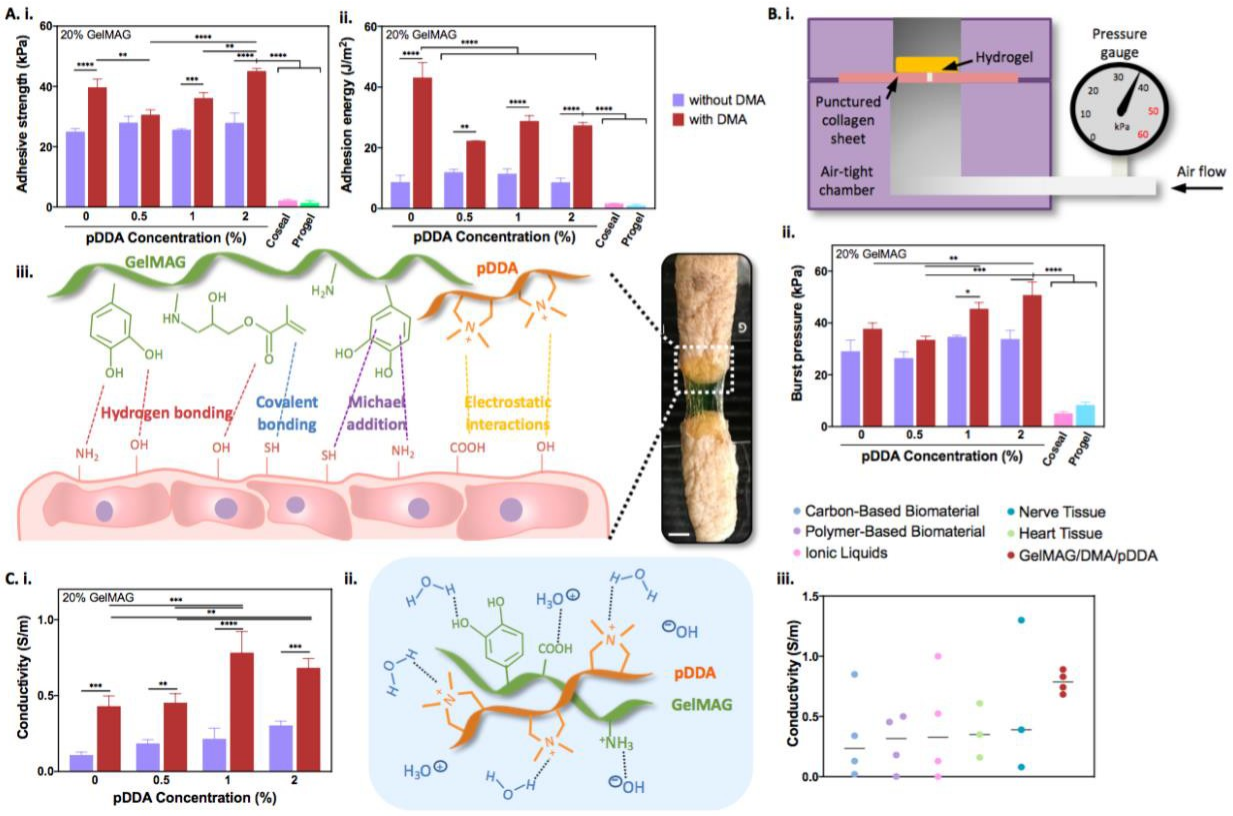

Figure 3. Adhesion and conductivity characterization of G/D/p hydrogel. (A) Wound closure on porcine skin tissue using GelMAG hydrogel samples with and without DMA and varying concentrations of pDDA quantified **(i.)** adhesion strength and **(ii.)** adhesion energy. Hydrogels measurements are compared to commercial sealants Coseal® and Progel™. **(iii.)** Schematic of chemical interactions between hydrogel moieties and biological surface. **(B)** Burst pressure test with **(i.)** customized set up quantified **(ii.)** burst pressure of all hydrogel compositions. Measurements were compared with commercial tissue sealants Coseal® and Progel™. **(C i.)** Ionic conductivity of all hydrogel samples. **(ii.)** Schematic of ionic conductance mechanism aqueous solution. **(iii.)** Comparative panel of conductivity of GelMAG/DMA/pDDA hydrogel compared to carbon-based biomaterial [54-57], polymer-based biomaterial [58-61], ionic liquids [62-66], as well as native cardiac [66] and nerve tissue [67]. Data are represented as mean ± SD (*P < 0.1, **P < 0.01, ***P < 0.001, ****P < 0.0001, N=4). Scale bar: 5 mm.

3.4 Antibacterial ability of GelMAG/DMA/pDDA hydrogel

The significant conductive property of the GelMAG hydrogel with DMA and pDDA imbues a multifunctional depth to the wound repair agent. As previously stated, open and slow-healing injuries commonly suffer from bacterial infections, which disrupt or lengthen the tissue repair timeline. Charged polymers like chitosan have been heavily utilized for hemostatic and wound healing ability, which arise from their strong conductive effect [68]. However, limitations of chitosan and saturation of research into this material calls for new developments in the field of polyelectrolyte-derived tissue engineering scaffolds. Quaternary ammonium-containing polymers like pDDA have widely been investigated for household antibacterial agents, but rarely for tissue engineering applications [69]. Therefore, the antibacterial ability of GelMAG hydrogels

containing DMA and pDDA were investigated for multifaceted bioengineering characterization (Fig. 4). The plethora of cation-saturated pDDA, even in 2% (v/v) of the total hydrogel composition acts, to attract and disrupt the negatively charged bacterial cell membranes of gram-negative *Pseudomonas aeruginosa* and gram-positive *Staphylococcus aureus* [69]. After incubation of all hydrogel conditions in bacterial suspension, we observed a decrease in bacterial viability of *P. aeruginosa* after just one day and a decrease in viability in the more prolific *S. aureus* after three days (Fig. 4A i-ii). Both strains of bacteria were more highly affected by hydrogels that contained pDDA. By day six of the bacterial viability assay, the *P. aeruginosa* control (without any hydrogel treatment) had grown to an optical density of 0.60 ± 0.003 and the pDDA-containing hydrogels averaged a density of 0.15 ± 0.01. Similarly, the *S. aureus* control proliferated to a density of 1.40 ± 0.01 while the pDDA-containing biomaterials averaged 0.45 ± 0.04. Both samples with higher concentrations of pDDA (GelMAG/2% pDDA and GelMAG/DMA/2% pDDA) exhibited fast and permanent bacterial defense, while both samples without pDDA (GelMAG and GelMAG/DMA) exhibited less bacterial growth than the control, but still had a notable density of 0.45 ± 0.04. Viability analysis for all hydrogels conditions was performed (Supplementary Fig. 7).

Bacterial viability was further detailed with colony forming unit analysis on day six of the viability assay in order to quantify the long-term bactericidal effect of the biomaterial (Fig. 4B). *P. aeruginosa* without hydrogel treatment grew to 519 ± 14 CFU while *S. aureus* grew to > 1000 CFU in the same time period (Fig. 4B i-ii). A similar result occurred when both strains of bacteria were treated with GelMAG hydrogel since GelMAG has no strong charge density – verified by zeta potential analysis – with which to initiate bacterial aggregation and cytoplasmic membrane disruption (Supplementary Fig. 7). However, when the bacteria were incubated with

GelMAG/DMA/2% pDDA hydrogel, the colony count of *P. aeruginosa* decreased to 274 ± 21 CFU and 286 ± 19 CFU for *S. aureus*. A visual portrayal of colony forming units of each hydrogel-treated bacteria strain is shown by agar plating (Fig. 4D). SEM imaging was performed on hydrogels after six days on incubation in bacterial suspension to further assess the antibacterial properties of the hydrogel surface (Fig. 4E). Compared to the GelMAG hydrogel that hosted numerous bacteria, the GelMAG/DMA/pDDA 2% hydrogel proved to be inhospitable for both the gram-positive and gram-negative bacteria. The rod-shaped P. aeruginosa (1-5 μm in length) and the spherical S. aureus (0.5-1.5 μL in diameter) are detailed.

A zone of inhibition test against both strains of bacteria was also conducted using the GelMAG and GelMAG/DMA/2% pDDA hydrogels (Fig. 4C). After one day of incubation, the GelMAG/DMA/pDDA 2% hydrogels created a 10 mm zone of inhibition when cultured with *P. aeruginosa* and a 7 mm zone of inhibition when cultured with *S. aureus* (Fig. 4C i-ii). Such strong antibacterial effect is caused by the leaching of unconjugated pDDA from the hydrogel matrix. The GelMAG hydrogel did not create a zone of inhibition against either strain of bacteria due to its lack of the essential polyelectrolyte. Nevertheless, the GelMAG/DMA/2% pDDA hydrogel offers potential as an antibacterial agent that will reduce the nosocomial infection-related complications without compromising mammalian cell viability.

Few biomaterials for wound treatment offer antimicrobial resistance. Our previously mentioned work with GelMA and GelMAC were not test for bactericidal ability since they do not contain components necessary for the chemical mechanisms by which the GelMAG/DMA/pDDA hydrogel kills bacteria. One such wound healing biomaterial that does possess antibacterial ability relies on chemically-modified chitosan, dopamine, and an acrylamide derivative [70]. Chitosan has predominantly been used for its antibacterial ability stemming from the highly charged

backbone, but it has previously mentioned limitations with biocompatibility. Additional incorporation of acrylamide also ensures risk of cytotoxicity, similar to other biomaterials that make use of synthetic polymers. Another work formulates an antibacterial hydrogel from zwitterionic polymer poly[2-(methacryloyloxy)ethyl]dimethyl-(3-sulfopropyl)ammonium hydroxide (polySMBA), quaternized chitosan methacrylate, and GelMA, which produce an inhospitable environment for bacteria, killing almost 100% of both strains tested [71]. The hydrogel also retains good tissue adhesion at roughly 40 kPa. However the material has insufficient tensile strength and extensibility to adapt to the dynamic environments of damaged tissue surfaces. On the other hand, our GelMAG/DMA/pDDA hydrogel retains effective long-term antibacterial ability to promote infection-free wound healing while still retaining other beneficial properties of a tissue engineering system.

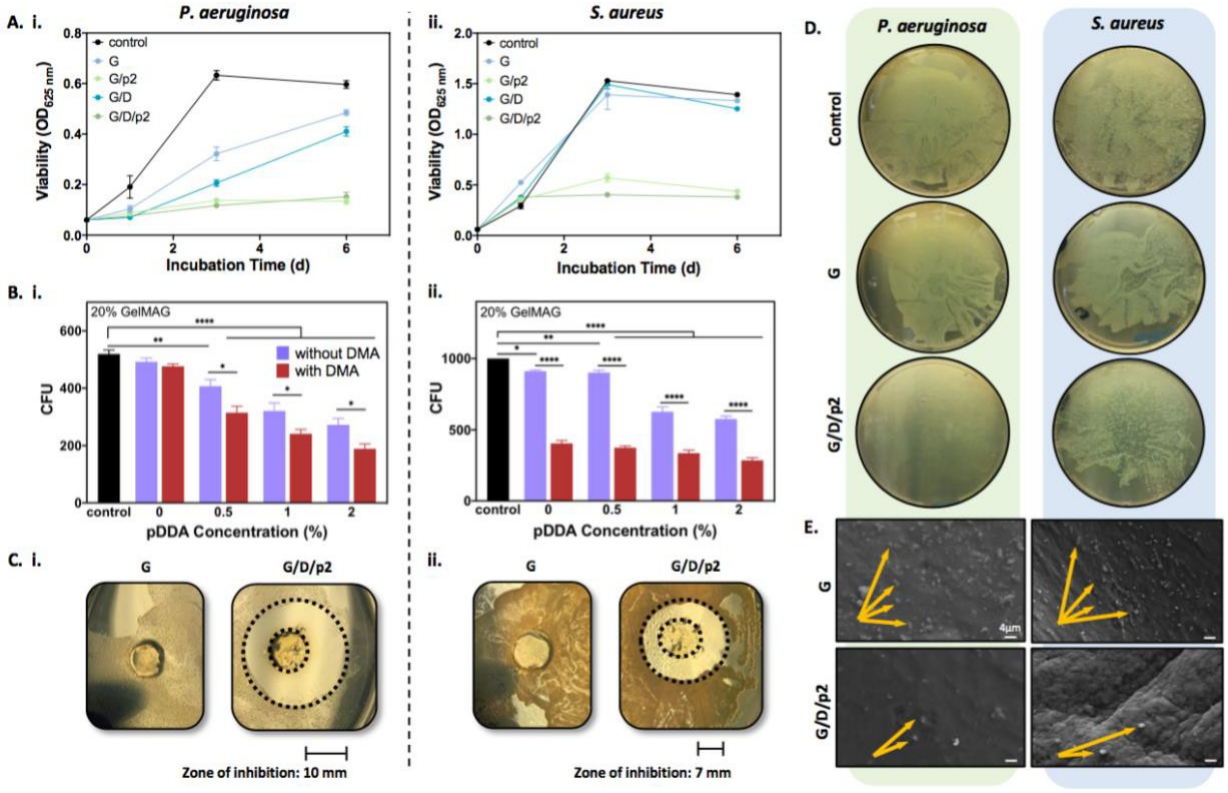

Figure 4. Antibacterial profile of G/D/p hydrogel. (A) Bacterial viability measured at 625 nm on **(i.)** *P. aeruginosa* and **(ii.)** *S. aureus* cultured that were treated with hydrogel. **(B)** Colony forming units of **(i.)** *P. aeruginosa* and **(ii.)** *S. aureus* after six days of incubation with hydrogel samples. **(C)** Zone of inhibition against **(i.)** *P. aeruginosa* and **(ii.)** *S. aureus* after culture with GelMAG and GelMAG/DMA/2% pDDA hydrogels. **(D)** Visual portrayal of CFU of both strains of bacteria after six days of incubation with GelMAG and GelMAG/DMA/2% pDDA. **(E)** SEM images of GelMAG and GelMAG/DMA/2% pDDA hydrogels after six days of incubation with bacteria. Scale bar: 4 μm. Control sample represents no biomaterial treatment. Data are represented as mean ± SD (*P < 0.1, **P < 0.01, ***P < 0.001, ****P < 0.0001, N=4).

3.5 Hemostatic ability of GelMAG/DMA/pDDA hydrogel

In addition to bacterial resistance, control of rapid bleeding is an essential ability of a biomaterial for wound healing potential. The mechanisms with which recently developed hemostatic biomaterials reduce blood loss often serve to compromise overall biocompatibility. For example, commercial hemostatic agents that employ silicon-based components such as zeolites and kaolinites provide quick hemorrhage control but are retarded due to the cytotoxicity of their silica-rich gel coating [72]. Furthermore, zeolites are characterized by thermal release and subsequently induce the risk of tissue burns during the hemostatic process [73]. Other common hemostatic agents make use of metals or synthetic polymers to attribute hemorrhage controlling ability, but these also present risk of compatibility at the cellular level [74-75]. Because our material was already characterized to possess strong conductive and antibacterial ability, it reserves the mechanism by which rapid hemostasis in enacted.

Therefore, extensive hemostatic testing was conducted to quantify this property (Fig. 5). Citrated fresh whole blood clotted in 58 ± 3 min (due to the diabetic condition of the blood donor), which was assessed both visually and through a quantitative hemoglobin absorption profile (Fig. 5A i, 5B). Whole blood hemoglobin absorbance was 1.20 ± 0.04 at the initial time point (20 min) and 0.02 ± 0.001 at the point of total cot formation (55 min) (Fig. 5C). When citrated blood was allowed to clot on top of the GelMAG hydrogel, clotting time decrease to 52 ± 3 min and further decreased to 38 ± 3 min upon addition of 2% pDDA to the GelMAG hydrogel. Hemoglobin absorbance from the GelMAG-treated sample dropped from an initial measurement of 0.38 ± 0.05 (20 min) to 0.12 ± 0.01 (50 min) and to 0.06 ± 0.005 for the GelMAG/2% pDDA-treated samples which coagulated at 40 minutes. The high cationic density of the polyelectrolyte forms electrostatic interactions with the predominantly negatively charged erythrocytes (Fig. A ii). On top of the hydrogen bonding interactions between the GelMAG amine, alcohol, and carboxyl groups and blood cells, pDDA enhances chemical interactions between the hemostatic agent and blood and consequently initiates faster blood coagulation. Upon conjugation of DMA to GelMAG, blood clots in 42 ± 3 min, confirmed by a hemoglobin absorbance of 0.02 ± 0.0003 at 40 min. The dopamine-derived moieties introduce more hydrogen bonding interactions as well as cation-pi interactions between the polymer and red blood cells. Erythrocytes have a dense inner layer of negative charge and a diffuse outer layer of both cationic and anionic charge. The cations comprising this diffuse layer interact with the electron-dense aromatic ring of DMA, which ultimately results in faster blood coagulation. Incorporating 2% pDDA into the GelMAG/DMA hydrogel further reduced blood clotting time to 30 ± 5 min, monitored by 0.02 ± 0.005 hemoglobin absorbance at 30 min. The addition of electrostatic interactions with the highly cationic polyelectrolyte and the predominantly anionic erythrocytes acted to improve the hemostatic

potential of the GelMAG/DMA/2% pDDA hydrogel. Clotting time and hemoglobin absorbance were assessed for all hydrogel compositions (Supporting Fig. 8, 9).

Clot weight measurement was analyzed at 20 minutes to determine how much clot had formed on top of each biomaterial sample at a preliminary point in the hemostatic test (Fig. 5D). GelMAG/DMA/2% pDDA showed superior hemostatic potential since it formed the heaviest clot at this initial time point. The blood clotting index of the GelMAG/DMA/2% pDDA hydrogel was reported to be 8 ± 4%, which further emphasizes the potential of the biomaterial to overcome hemorrhage (Fig. 5E). Additionally, the GelMAG/DMA/2% pDDA hydrogel has high and fast swelling ability. The biomaterial swells to a maximum of 345 ± 40% within the first four hours of submersion in an aqueous solution (Supplementary Fig. 10). Rapid blood uptake into the polymer matrix would provide the advantages of faster clot formation and minimal blood loss.

Recently developed bioadhesives offer multifunctionality through antimicrobial effect, self-healing, or cellular infiltration effect, but few biocompatible systems offer the advantage of effective reduction of blood loss. [76] Our previous work done with GelMAC has hemostatic ability but is only able to reduce blood clotting time by 40% while lacking aforementioned mechanical properties suitable for wound healing [41]. Another work with hyaluronic acid functionalized with catechol and combined with PEG succeeds in reducing blood clotting time by 50% but is characterized by disadvantageous properties with a Youngs modulus of 20 kPa and an adhesion strength under 15 kPa, which makes the gastrointestinal hemorrhage device susceptible to mechanical or adhesive failure [77]. Our material retains adequate stretchability and adhesion to tissue systems while reducing blood clotting time by 50% and ultimately expediting the major step towards wound healing: hemostasis.

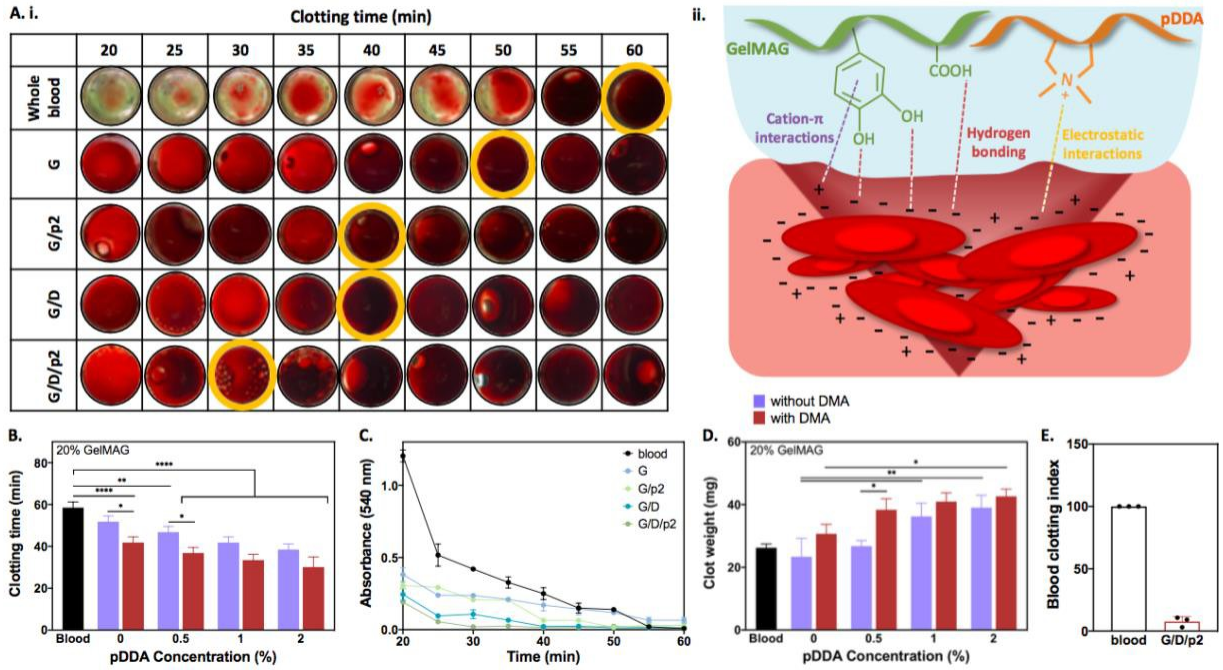

Figure 5. Hemostatic profile of G/D/p hydrogel. (A i.) Clotting time of citrated fresh whole blood on various hydrogel conditions. **(ii.)** Schematic of the chemical mechanisms of blood coagulation under hydrogel treatment. **(B)** Quantitative representation of clotting time. **(C)** Absorbance of hemoglobin measured at 540 nm for hydrogel-treated blood samples that were quenched with PBS to stop blood coagulation. **(D)** Clotting weight of hydrogel-treated blood at 20 minutes of hemostatic test. **(E)** Blood clotting index of GelMAG/DMA/2% pDDA hydrogel compared to whole blood. Data are represented as mean ± SD (*P < 0.1, **P < 0.01, ***P < 0.001, ****P < 0.0001, N=4).

3.6 In vitro biocompatibility of GelMAG/DMA/pDDA hydrogel

Biocompatibility is emphasized as a primary benefit of our hydrogel. As previous stated, biomaterials for injury treatment come in numerous forms with a wide range of benefits and disadvantages. An overwhelming disadvantage for materials promising robust adhesion to the injured tissue or rapid hemostasis to accelerate wound healing is cellular toxicity. Chemical

modification or blending of a composite using synthetically-derived polymers and cytotoxic components may result in a decrease of cellular viability and proliferation. This immediately impedes application of the biologically-incompatible material. Therefore, cellular biocompatibility assays were conducted on our hydrogel material using embryonic mouse fibroblast (3T3) cells to ensure safety of use in living systems (Fig. 6). Live/dead staining was conducted on GelMAG and GelMAG/DMA/2% pDDA hydrogels with a control of no hydrogel treatment in order to determine cell viability at one and five of the culture (Fig. 6A i). The cells stained with membrane-permeant green fluorescent dye indicate live cells while cells stained red in their plasma membranes indicate dead cells. Both hydrogels show comparable intensity of green fluorescence and similar cell viability compared to each other and to the hydrogel-free control at all time points, all averaging 96 ± 1% viability (Fig. 6B). Actin/DAPI staining was also conducted to assess cell morphology after one and five days of treatment with GelMAG and GelMAG/DMA/2% pDDA hydrogels. The green-dyed actin filaments and blue-dyed nuclei portrayed cellular attachment and proliferation (Fig. 6A ii). Healthy morphology was indicated by the elongated shape of the green-dyed actin. The amounts of cells per square millimeter at day one of the assay increases from 153 ± 35 cells/mm^2 in the control sample to 309 ± 35 cells/mm^2 in the GelMAG/DMA/2% pDDA hydrogel (Fig. 6C). There is a significant increase in cell count at day five of the assay, indicating healthy proliferation at an average of 1946 ± 89 cells/mm^2 for all tested conditions. Metabolic activity of cells cultured with hydrogels was also analyzed using a PrestoBlue assay on days one, three, and five of the assay. An increase in the relative fluorescence of the PrestoBlue reagent at 570 nm from 1454 ± 21 at day one to 9843 ± 139 at day five indicates a steady increase in metabolic activity within the cells. Hence the biocompatibility was confirmed for the GelMAG/DMA/pDDA hydrogel that provides multifaceted and biologically safe assistance for wound healing. In addition

to biocompatibility, the hydrogels also maintain biodegradability at a physiologically relevant speed for tissue repair, which eliminates the need for medical removal of the biomaterial (Supporting Fig. 11).

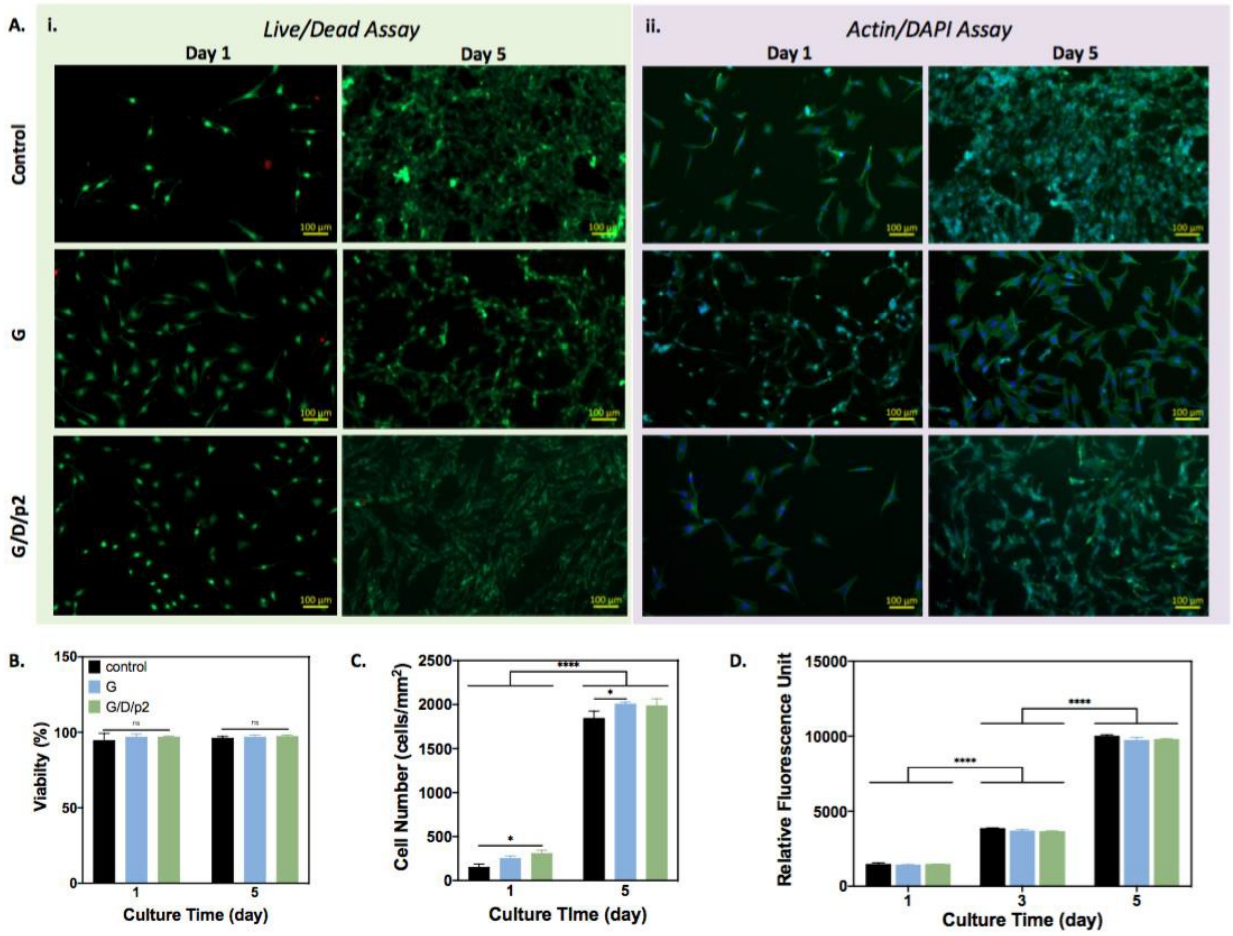

Figure 6. In vitro biocompatibility of G/D/p hydrogel. (A) Representative images of live/dead and actin/DAPI staining assays on mouse embryonic fibroblast (3T3) cells cultured with GelMAG and GelMAG/DMA/pDDA 2% hydrogels with no hydrogel presence used as a control. Scale bar: 100 µm. **(B)** 3T3 cell viability after cultured with hydrogels for one and five days. **(C)** 3T3 cell proliferation when cultured with hydrogels for one and five days. **(D)** Metabolic activity after culture with hydrogels after one, three, and five days using a PrestoBlue assay. Data are represented as mean ± SD (*P < 0.1, **P < 0.01, ***P < 0.001, ****P < 0.0001, N=3).

CHAPTER IV. Conclusion

In this study, we developed an elastic, adhesive, conductive, antimicrobial, and hemostatic biomaterial for the treatment of hemorrhage. Optimization of material synthesis granted the hydrogel with the mechanical properties necessary to mimic a cellular microenvironment upon which tissue engineering would occur. The GelMAG hydrogel with conjugated DMA and incorporated pDDA showed high elasticity (~ 200%), which is necessary of a biomaterial that will be used on a dynamic and motive surface such as skin. The hydrogel also experiences a minimal loss of energy upon cyclic compression, so it can withstand continuous amounts of strain without deformation. This fact is especially vital since many internal organs on which hemostatic biomaterials are used undergo expansion and contraction (ex. lung, heart), so a material that retains stretchability and compression energy minimizes risk of detachment or distortion before adequate wound healing. The GelMAG/DMA/pDDA hydrogel maintains robust adhesion to native tissue, which is an essential characteristic of an effective hemostatic agent. Mussel-inspired adhesion mechanisms that employ catechol-based conjugations cause a high adhesion strength (~ 45 kPa) on porcine skin tissue and high burst pressure (~ 51 kPa) on collagen sheet, significantly higher than commercial hemostatic and tissue sealant products Coseal and Progel. Further characterization of the hydrogel system revealed a high conductivity (~ 0.80 S/m) that is within the range of native heart and nerve tissue and exceeds the conductivity range of several carbon, polymer, and ionic liquid-based biomaterials for medicinal application. The mechanism of ionic conductivity underlies the antimicrobial property exemplified by the GelMAG/DMA/pDDA hydrogel. The polymer system shows a bactericidal effect against gram-negative and gram-positive strains of bacteria. The polyelectrolyte pDDA that is not conjugated to the polymer matrix leaches out of the hydrogel when submerged in aqueous solution, and this positively-charged

polymer caused further antibacterial resistance by creating a substantial zone of inhibition. The mechanism of conductivity and antibacterial resistance sheds light on the notable hemostatic ability of the hydrogel biomaterial. GelMAG/DMA/pDDA reduces blood clotting time of whole blood in half due primarily to the charge interactions between erythrocytes and components of the hydrogel. Lastly, in vitro biocompatibility assays showcase the biocompatibility of the hydrogel system. Although further in vivo and ex vivo tests must be done to prove biodegradability and effectivity, the developed biocompatible and multifunctional hydrogel exhibits potential to combat uncontrollable bleeding that surpasses traditional methods of hemorrhage control. In addition to hemorrhage treatment, the conductive and biocompatible nature of GelMAG/DMA/pDDA make for an effective nerve guidance conduit. Electrical communication between nerve cells has been proven to enhance nerve tissue regeneration, so a biopolymer that can mimic the cellular microenvironment and promote signaling without compromising innocuous physiological conditions can offer beneficial tissue regenerative ability. Nerve tissue is especially in need of conjugates to alleviate cells of the stress of regeneration since nerve cells are both slow and sensitive to grow back after cell injury or death [78]. Cardiac tissue is another that exploits external conductance to promote injured tissue regeneration. In cases of myocardial infarction, for example, infarcted tissue faces resistance in repairing correctly such that further medical complications like maladaptive ventricular remodeling does not occur [79]. Further applications of the GelMAG/DMA/pDDA hydrogel therefore include the regeneration of electroactive tissue such as nerve, heart, and muscle tissue.

APPENDIX

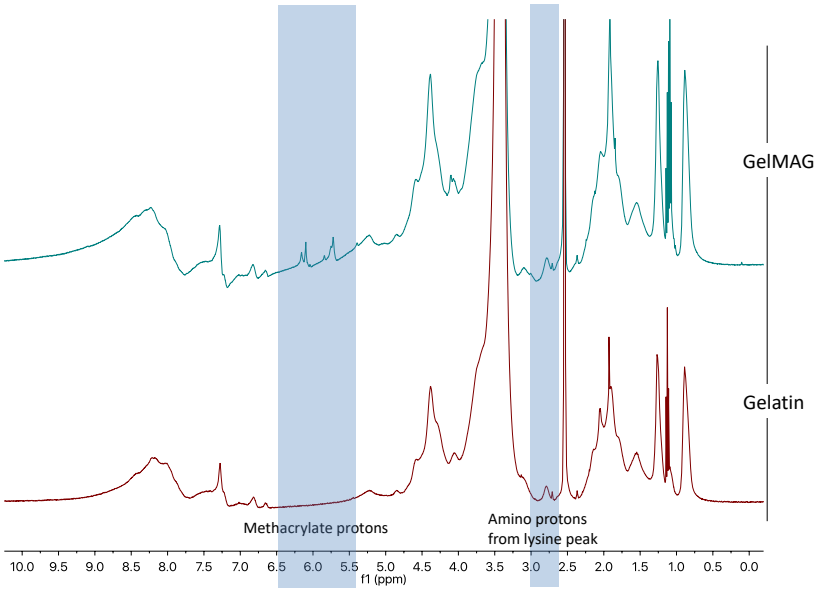

Supplementary Figure 1. ^{1}H NMR of gelatin and GelMAG. Peaks corresponding to the methacrylate protons are highlighted to show success of methacrylation reaction. And lysine peaks are highlighted to show which curve is integrated to determine degree of methacrylation.

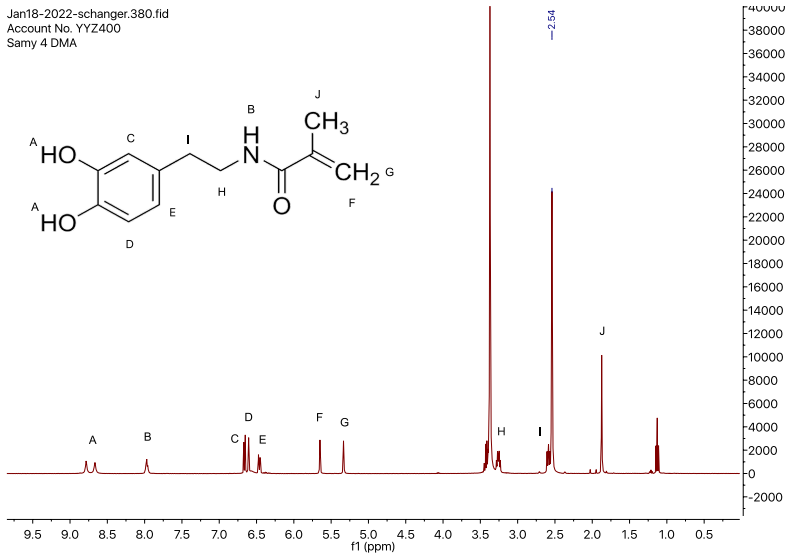

Supplementary Figure 2. ^{1}H NMR of DMA. Peaks corresponding to each proton on DMA is detailed.

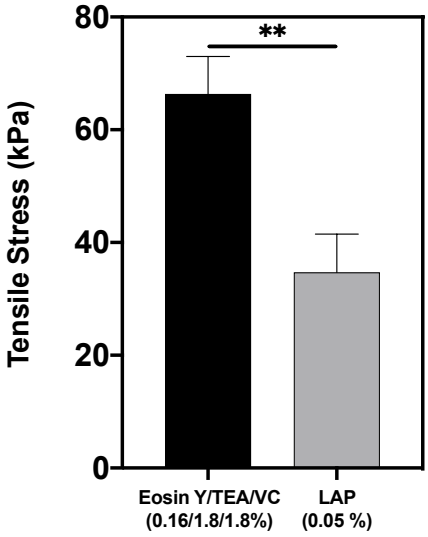

Supplementary Figure 3. Tensile stress of GelMAG hydrogel when prepared using EosinY/TEA/VC and LAP photoinitiator.

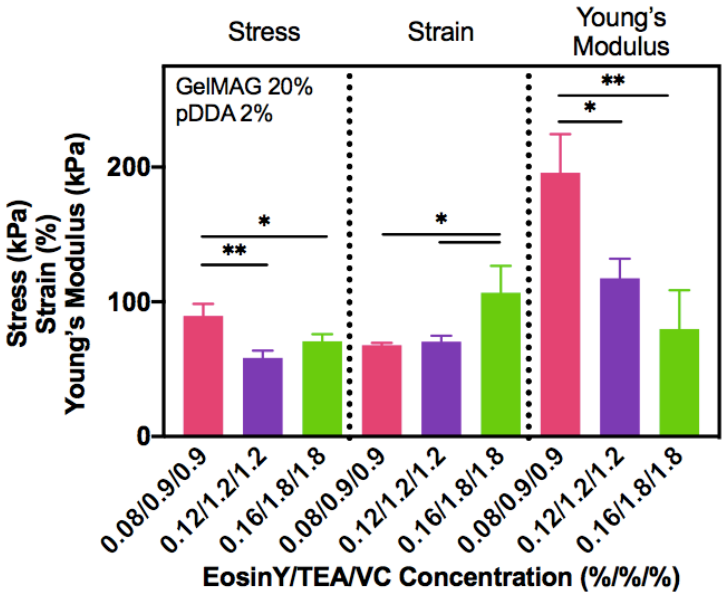

Supplementary Figure 4. Tensile stress, strain, and Young's modulus on GelMAG hydrogel containing 2.5% pDDA prepared in different concentrations of photoinitiator solution.

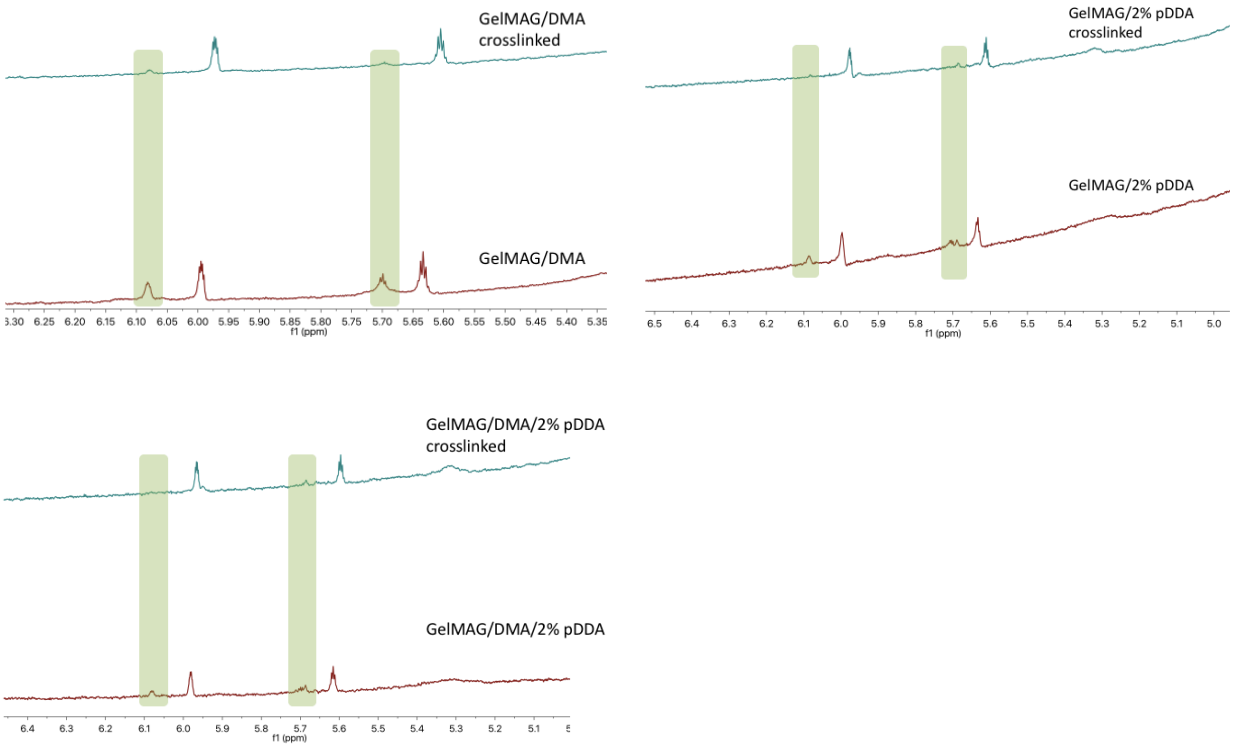

Supplementary Figure 5. ^{1}H NMR analysis of prepolymer and crosslinked samples containing GelMAG/DMA (top left), GelMAG/2% pDDA (top right), and GelMAG/DMA/2% pDDA (bottom left). Consumption of methacryloyl protons at 5.70 ppm and 6.08 ppm were monitored to assess crosslinking degree.

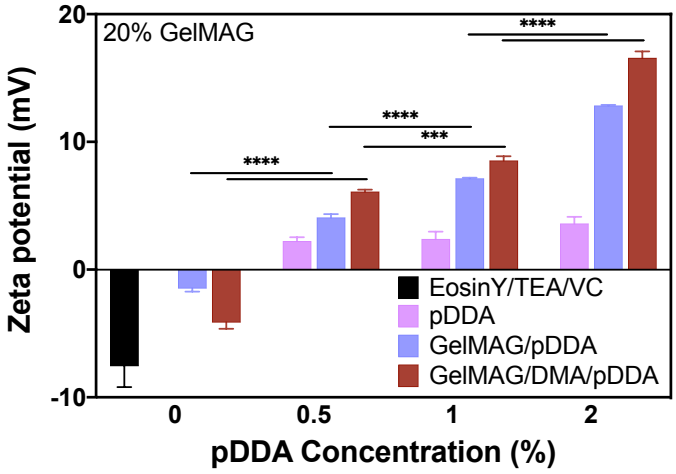

Supplementary Figure 6. Zeta potential analysis of charge density of GelMAG prepolymer solutions with and without both DMA and pDDA. The solutions were prepared and measured in Eosin Y/TEA/VC.

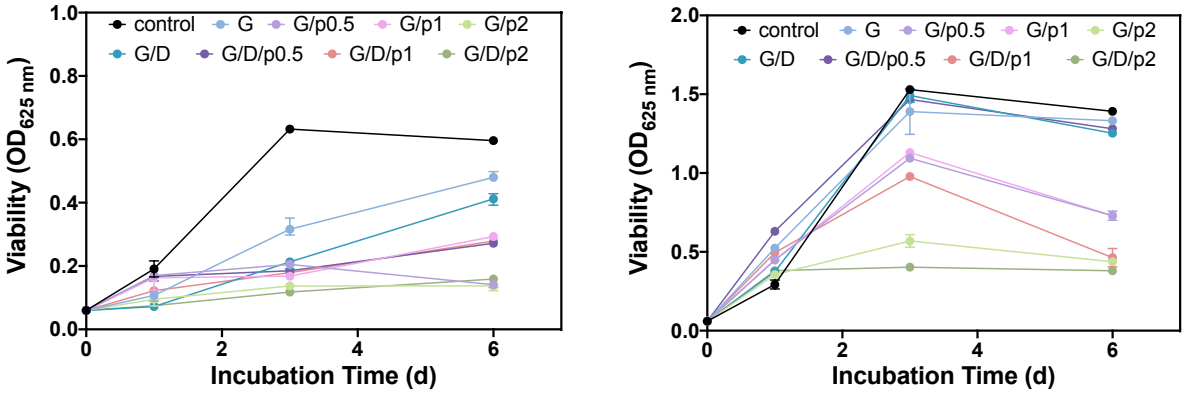

Supplementary Figure 7. Bacterial survival testing with optical density measurements at 625 nm. Bacteria tested is *Pseudomonas aeruginosa* (left) and *Staphylococcus aureus* (right).

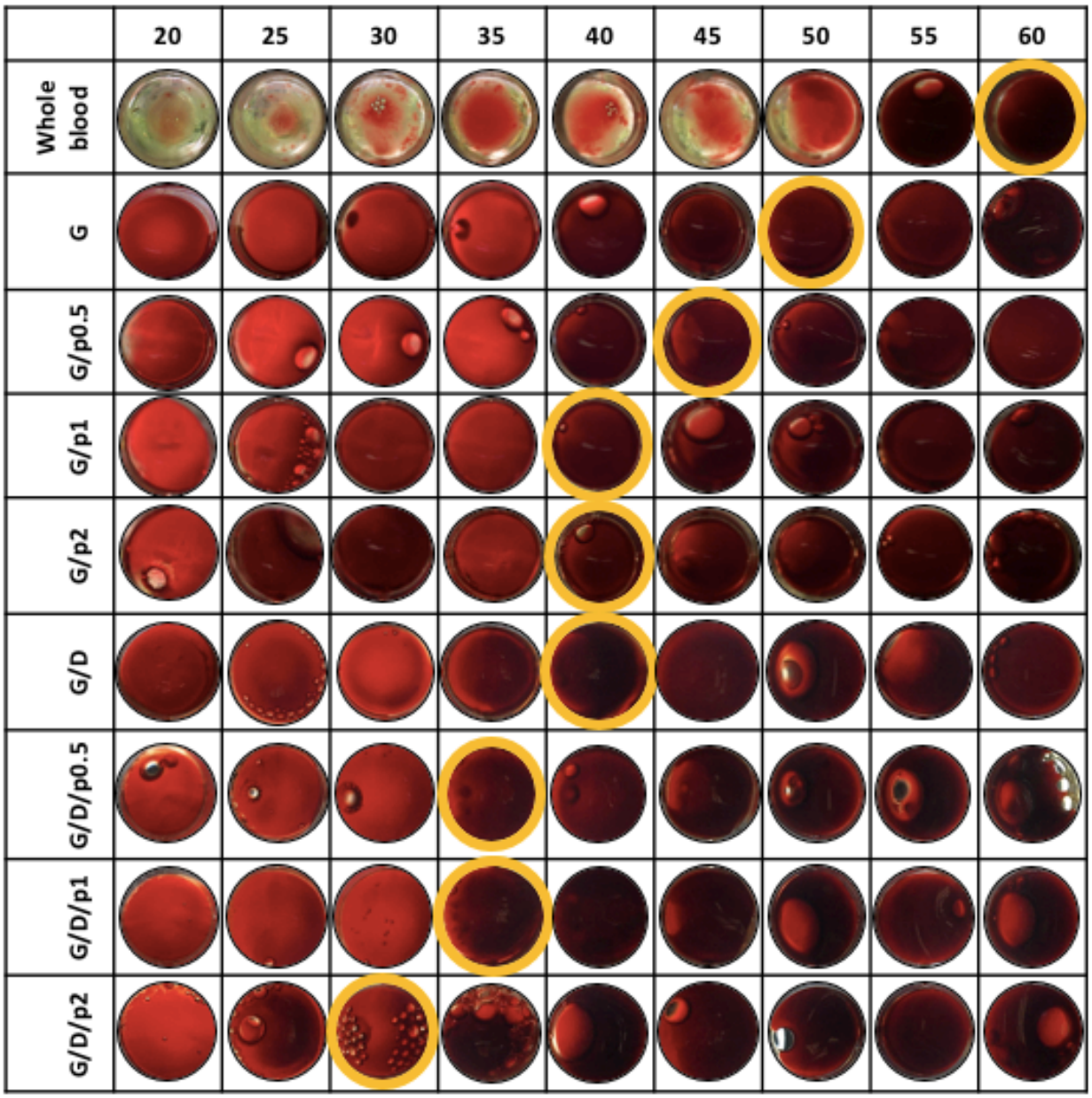

Supplementary Figure 8. Hemostatic test using citrated whole blood and analyzing clotting time on all GelMAG hydrogel conditions with and without both DMA and varying concentrations of pDDA.

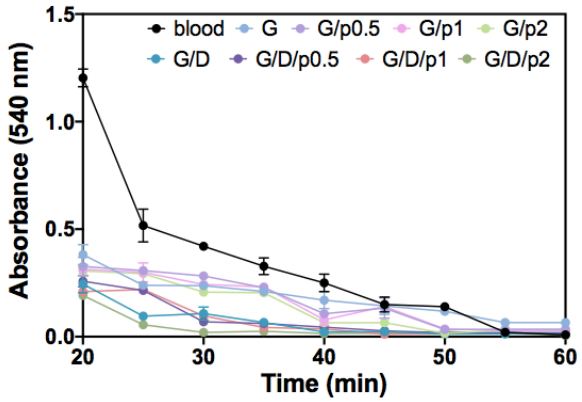

Supplementary Figure 9. Hemoglobin absorbance at 540 nm to accompany hemostatic testing of all hydrogel sample conditions.

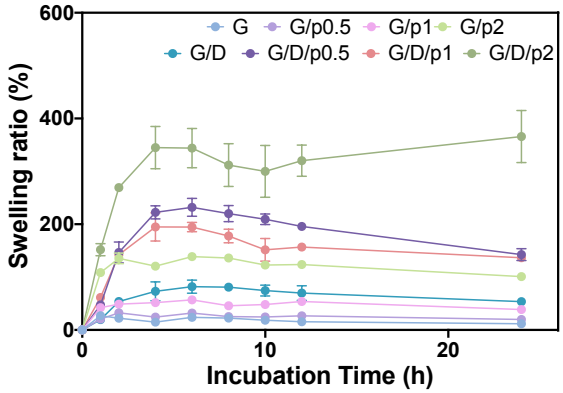

Supplementary Figure 10. Swelling ratio was taken of hydrogels incubated in PBS solution.

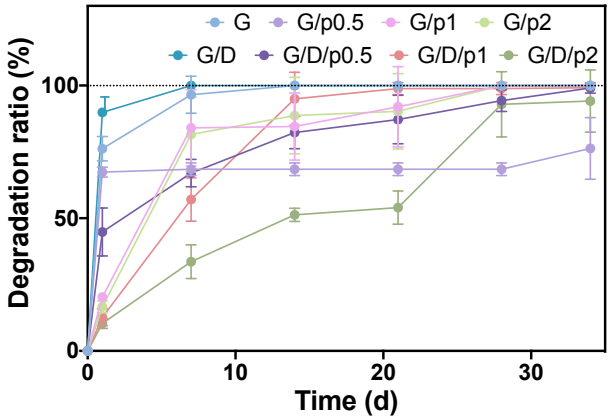

Supplementary Figure 11. Degradation profile was taken of hydrogels incubated in 2U/ml collagenase (type II) solution at a temperature of 37˚C for a period of 34 days.

BIBLIOGRAPHY

1. 2021. “Injuries and Violence.” World Health Organization. https://www.who.int/news-room/fact-sheets/detail/injuries-and-violence
2. K. J. Kalkwarf et al. “Bleeding to death in a big city: An analysis of all trauma deaths from hemorrhage in a metropolitan area during 1 year.” J Trauma Acute Care Surg 89, 716-722 (2020). DOI: 10.1097/TA.0000000000002833
3. J. L. Bienstock, A. C. Eke, N. A. Hueppchen. “Postpartum Hemorrhage.” N Engl J Med 384, 1635-1645 (2021). DOI: 10.1097/TA.0000000000002833
4. D. S. Kauvar, R. Lefering, C. E. Wade. “Impact of hemorrhage on trauma outcome: an overview of epidemiology, clinical presentations, and therapeutic considerations.” J Trauma 60, S3-11 (2006). DOI; 10.1097/01.ta.0000199961.02677.19
5. F. Fan, S. Saha, D. Hanjaya-Putra. “Biomimetic Hydrogels to Promote Wound Healing.” Front Bioeng Biotechnol 9, 718377 (2021). DOI: 10.3389/fbioe.2021.718377
6. A. Grover, A. Singh, D. S. Sidhu. “A Prospective Randomized Trial of Open Wound Treatment vs Occlusive Dressings in Elective Surgical Cases with Respect to Surgical Site Infections.” J Clin Diagn Res 9, PC26-29 (2015). DOI: 10.7860/JCDR/2015/13431.6105
7. “Bacterial Infection Symptoms: Signs and Treatment.” Medical News Today, MediLexicon International, https://www.medicalnewstoday.com/articles/bacterial-infection-symptoms#:~:text=Any%20severe%20or%20untreated%20bacterial,fever%20or%20chills.
8. Public Health, Epidemiology. “Diseases & Topics.” NC DPH: Healthcare-Associated Infections (HAIs), https://epi.dph.ncdhhs.gov/cd/diseases/hai.html.
9. A. J. Gale. “Continuing education course #2: current understanding of hemostasis.” Toxicol Pathol 39, 273-280 (2011). DOI: 10.1177/0192623310389474

10. H. T. Peng. “Hemostatic agents for prehospital hemorrhage control: a narrative review.” Mil Med Res 7, 13 (2020). DOI: 10.1186/s40779-020-00241-z

11. M. K. Jankite. “Blood Transfusion: Cost, Quality, and Other Considerations for the Surgical Management of the Critically Ill.” Crit Care Nurs Q 42, 173-176 (2019). DOI: 10.1097/CNQ.0000000000000250

12. Shander, A., et al. “Activity-Based Costs of Plasma Transfusions in Medical and Surgical Inpatients at a US Hospital.” Vox Sanguinis 111, 55–61 (2016). DOI: 10.1111/vox.12386

13. P. Rocha, M. Carvalho, M. Lopes, F. Araújo. “Costs and utilization of treatment in patients with hemophilia.” BMC Health Serv Res 15, 484 (2015). DOI: 10.1186/s12913-015-1134-3

14. A. Ockerman et al. “Tranexamic acid for the prevention and treatment of bleeding in surgery, trauma and bleeding disorders: a narrative review.” Thromb J 19, 54 (2021). DOI: 10.1186/s12959-021-00303-9

15. A. Girish et al. “Trauma-targeted delivery of tranexamic acid improves hemostasis and survival in rat liver hemorrhage model.” J Thromb Haemost 17, 1632-1644 (2019). DOI: 10.1111/jth.14552

16. “Using Topical Hemostatic Agents.” NATA, 6 Jan. 2017, https://www.nata.org/blog/beth-sitzler/using-topical-hemostatic-agents.

17. I. Otrocka-Domagała et al. “Safety of the long-term application of QuikClot Combat Gauze, ChitoGauze PRO and Celox Gauze in a femoral artery injury model in swine - a preliminary study.” Pol J Vet Sci 19, 337-343 (2016). DOI: 10.1515/pjvs-2016-0041

18. A. Simpson, A. Shukla, A. C. Brown. “Biomaterials for Hemostasis.” Annu Rev Biomed Eng 24, 111-135 (2022). DOI: 10.1146/annurev-bioeng-012521-101942

19. D. Li et al. “Recent Advances on Synthetic and Polysaccharide Adhesives for Biological Hemostatic Applications.” Front Bioeng Biotechnol 8, 926 (2020). DOI: 10.3389/fbioe.2020.00926

20. Pediatric Education. “What Are the Pros and Cons to Different Wound Closure Devices?: Pediatric Case and Reference Article.” Pediatric Education (2009). https://pediatriceducation.org/2009/09/21/what-are-the-pros-and-cons-to-different-wound-closure-devices/.

21. J. Sung, D. G. Lee, S. Lee, J. Park, H. W. Jung. “Crosslinking Dynamics and Gelation Characteristics of Photo- and Thermally Polymerized Poly(Ethylene Glycol) Hydrogels.” Materials (Basel) 13, (2020). DOI: 10.3390/ma13153277

22. “Ultraviolet (UV) Radiation.” American Cancer Society, https://www.cancer.org/healthy/cancer-causes/radiation-exposure/uv-radiation.html#:~:text=Exposure%20to%20UV%20rays%20can,to%20become%20inflamed%20or%20burned.

23. C. Borek. “Antioxidants and radiation therapy.” J Nutr 134, 3207S-3209S (2004). DOI: 10.1093/jn/134.11.3207S

24. R. H. Fortelny et al. “Cyanoacrylate tissue sealant impairs tissue integration of macroporous mesh in experimental hernia repair.” Surg Endosc 21, 1781-1785 (2007). DOI: 10.1007/s00464-007-9243-7

25. Trott, Alexander T. “Cyanoacrylate Tissue Adhesives.” JAMA, vol. 277, no. 19, 1997, p. 1559., https://doi.org/10.1001/jama.1997.03540430071037. DOI: 10.1001/jama.1997.03540430071037

26. K. M. Lewis, H. Atlee, A. Mannone, L. Lin, A. Goppelt. “Efficacy of hemostatic matrix and microporous polysaccharide hemospheres.” J Surg Res 193, 825-830 (2015). DOI: 10.1016/j.jss.2014.08.026

27. Q. He et al. “Positive charge of chitosan retards blood coagulation on chitosan films.” J Biomater Appl 27, 1032-1045 (2013). DOI: 10.1177/0885328211432487

28. M. Yin et al. “Novel quaternarized N-halamine chitosan and polyvinyl alcohol nanofibrous membranes as hemostatic materials with excellent antibacterial properties.” Carbohydr Polym 232, 115823 (2020). DOI: 10.1016/j.carbpol.2019.115823

29. J. Cheng et al. “Hydrogel-Based Biomaterials Engineered from Natural-Derived Polysaccharides and Proteins for Hemostasis and Wound Healing.” Front Bioeng Biotechnol 9, 780187 (2021). DOI: 10.3389/fbioe.2021.780187

30. X. Huang et al. “Surface roughness of silk fibroin/alginate microspheres for rapid hemostasis in vitro and in vivo.” Carbohydr Polym 253, 117256 (2021). DOI: 10.1016/j.carbpol.2020.117256

31. N. Annabi et al. “Engineering a sprayable and elastic hydrogel adhesive with antimicrobial properties for wound healing.” Biomaterials 139, 229-243 (2017). DOI: 10.1016/j.biomaterials.2017.05.011

32. J. Sun et al. “Fabrication and Mechanical Properties of Engineered Protein-Based Adhesives and Fibers.” Adv Mater 32, e1906360 (2020). DOI: 10.1002/adma.201906360

33. H. Yuk et al. “Dry double-sided tape for adhesion of wet tissues and devices.” Nature 575, 169-174 (2019). DOI: 10.1038/s41586-019-1710-5

34. L. M. Sanches, D. F. Petri, L. D. de Melo Carrasco, A. M. Carmona-Ribeiro “The antimicrobial activity of free and immobilized poly (diallyldimethylammonium) chloride in

nanoparticles of poly (methylmethacrylate).” J Nanobiotechnology 13, 58 (2015). DOI: 10.1186/s12951-015-0123-3

35. D. Gan et al. “Mussel-inspired dopamine oligomer intercalated tough and resilient gelatin methacryloyl (GelMA) hydrogels for cartilage regeneration.” J Mater Chem B 7, 1716-1725 (2019). DOI: 10.1039/c8tb01664j
36. I. Noshadi et al. “In vitro and in vivo analysis of visible light crosslinkable gelatin methacryloyl (GelMA) hydrogels.” Biomater Sci 5, 2093-2105 (2017). DOI: 10.1039/c7bm00110j
37. K. Yue et al. “Synthesis, properties, and biomedical applications of gelatin methacryloyl (GelMA) hydrogels.” Biomaterials 73, 254-271 (2015). DOI: 10.1016/j.biomaterials.2015.08.045
38. N. Annabi, K. Yue, A. Tamayol, A. Khademhosseini, Elastic sealants for surgical applications. Eur J Pharm Biopharm 95, 27-39 (2015). DOI: 10.1016/j.ejpb.2015.05.022
39. M. H. Murdock et al., Cytocompatibility and mechanical properties of surgical sealants for cardiovascular applications. J Thorac Cardiovasc Surg 157, 176-183 (2019). DOI: 10.1016/j.jtcvs.2018.08.043
40. A. Assmann et al., A highly adhesive and naturally derived sealant. Biomaterials 140, 115-127 (2017). DOI: 10.1016/j.biomaterials.2017.06.004
41. S. Baghdasarian et al. “Engineering a naturally derived hemostatic sealant for sealing internal organs.” Mater Today Bio 13, 100199 (2022). DOI: 10.1016/j.mtbio.2021.100199
42. A. H. J. Gowda et al. “Design of tunable gelatin-dopamine based bioadhesives.” Int J Biol Macromol 164, 1384-1391 (2020). DOI: 10.1016/j.ijbiomac.2020.07.195

43. E. Shirzaei Sani et al., Sutureless repair of corneal injuries using naturally derived bioadhesive hydrogels. Sci Adv 5, eaav1281 (2019). DOI: 10.1126/sciadv.aav1281

44. Pei, Xinjie, et al. "Recent Progress in Polymer Hydrogel Bioadhesives." Journal of Polymer Science 59, 1312–1337 (2021). DOI: 10.1002/pol.20210249

45. H. Montazerian et al. "Stretchable and Bioadhesive Gelatin Methacryloyl-Based Hydrogels Enabled by in Situ Dopamine Polymerization." ACS Appl Mater Interfaces 13, 40290-40301 (2021). DOI: 10.1021/acsami.1c10048

46. H. Lee, N. F. Scherer, P. B. Messersmith. "Single-molecule mechanics of mussel adhesion." Proc Natl Acad Sci U S A 103, 12999-13003 (2006). DOI: 10.1073/pnas.0605552103

47. C. Zhang et al. "Revisiting the adhesion mechanism of mussel-inspired chemistry." Chem Sci 13, 1698-1705 (2022). DOI: 10.1039/d1sc05512g

48. Gordon, Terry L, and Martin E Fakley. "The Influence of Elastic Modulus on Adhesion to Thermoplastics and Thermoset Materials." International Journal of Adhesion and Adhesives 23, 95–100 (2003). DOI: 10.1016/s0143-7496(02)00064-7

49. Lane, Michael, et al. "Plasticity Contributions to Interface Adhesion in Thin-Film Interconnect Structures." Journal of Materials Research 15, 2758–2769 (2000). DOI: 10.1557/jmr.2000.0395.

50. Han, Lu, et al. "Tough, Self-Healable and Tissue-Adhesive Hydrogel with Tunable Multifunctionality." NPG Asia Materials 9, (2017). DOI: 10.1038/am.2017.33

51. K. Zhang et al., Efficient catechol functionalization of biopolymeric hydrogels for effective multiscale bioadhesion. Mater Sci Eng C Mater Biol Appl 103, 109835 (2019). DOI: 10.1016/j.msec.2019.109835

52. Xie, Lei, et al. “A Wet Adhesion Strategy via Synergistic Cation–π and Hydrogen Bonding Interactions of Antifouling Zwitterions and Mussel-Inspired Binding Moieties.” Journal of Materials Chemistry A 7, 21944–21952 (2019). DOI: 10.1039/C9TA08152F

53. K. Han et al. “Gelatin-based adhesive hydrogel with self-healing, hemostasis, and electrical conductivity.” Int J Biol Macromol 183, 2142-2151 (2021). DOI: 10.1016/j.ijbiomac.2021.05.147

54. W. Zhang, F. K. Yang, Z. Pan, J. Zhang, B. Zhao. “Bio-inspired dopamine functionalization of polypyrrole for improved adhesion and conductivity.” Macromol Rapid Commun 35, 350-354 (2014). DOI: 10.1002/marc.201300761

55. P. Baei et al. “Electrically conductive gold nanoparticle-chitosan thermosensitive hydrogels for cardiac tissue engineering.” Mater Sci Eng C Mater Biol Appl 63, 131-141 (2016).

56. Y. Wang et al. “Conductive graphene oxide hydrogels reduced and bridged by l-cysteine to support cell adhesion and growth.” J Mater Chem B 5, 511-516 (2017).

57. C. Arndt et al. “Microengineered Hollow Graphene Tube Systems Generate Conductive Hydrogels with Extremely Low Filler Concentration.” Nano Lett 21, 3690-3697 (2021).

58. B. S. Eftekhari, M. Eskandari, P. A. Janmey, A. Samadikuchaksaraei, M. Gholipourmalekabadi. “Conductive chitosan/polyaniline hydrogel with cell-imprinted topography as a potential substrate for neural priming of adipose derived stem cells.” RSC Adv 11, 15795-15807 (2021).

59. Chalmers, Evelyn, et al. “Increasing the Conductivity and Adhesion of Polypyrrole Hydrogels with Electropolymerized Polydopamine.” Chemistry of Materials 32, 234-244 (2019). DOI: 10.1021/acs.chemmater.9b03655

60. Wang, Shen, et al. “Fabrication of Polypyrrole-Grafted Gelatin-Based Hydrogel with Conductive, Self-Healing, and Injectable Properties.” ACS Applied Polymer Materials 2, 3016-3023 (2020). DOI: 10.1021/acsapm.0c00468
61. J. Yang, G. Choe, S. Yang, H. Jo, J. Y. Lee. “Polypyrrole-incorporated conductive hyaluronic acid hydrogels.” Biomater Res 20, 31 (2016).
62. I. Noshadi et al. “Engineering Biodegradable and Biocompatible Bio-ionic Liquid Conjugated Hydrogels with Tunable Conductivity and Mechanical Properties.” Sci Rep 7, 4345 (2017).
63. Meira, R. M., et al. “Ionic-Liquid-Based Electroactive Polymer Composites for Muscle Tissue Engineering.” ACS Applied Polymer Materials 1, 2649-2658 (2019). DOI: 10.1021/acsapm.9b00566
64. Wang, Wenwu, et al. “Conductive Ionic Liquid/Chitosan Hydrogels for Neuronal Cell Differentiation.” Engineered Regeneration 3, 1–12 (2022). DOI: 10.1016/j.engreg.2022.01.007
65. B. Blessing et al. “The Impact of Composition and Morphology on Ionic Conductivity of Silk/Cellulose Bio-Composites Fabricated from Ionic Liquid and Varying Percentages of Coagulation Agents.” Int J Mol Sci 21, (2020).
66. K. Raghavan et al. “Electrical conductivity and permittivity of murine myocardium.” IEEE Trans Biomed Eng 56, 2044-2053 (2009).
67. J. H. Lee et al. “In vivo electrical conductivity measurement of muscle, cartilage, and peripheral nerve around knee joint using MR-electrical properties tomography.” Sci Rep 12, 73 (2022).

68. Z. Hu, D. Y. Zhang, S. T. Lu, P. W. Li, S. D. Li. “Chitosan-Based Composite Materials for Prospective Hemostatic Applications.” Mar Drugs 16, (2018). DOI: 10.3390/md16080273

69. Hora, Priya I., et al. “Increased Use of Quaternary Ammonium Compounds during the SARS-COV-2 Pandemic and beyond: Consideration of Environmental Implications.” Environmental Science & Technology Letters 7, 622–631 (2020). DOI: 10.1021/acs.estlett.0c00437

70. W. Han et al. “Biofilm-inspired adhesive and antibacterial hydrogel with tough tissue integration performance for sealing hemostasis and wound healing.” Bioact Mater 5, 768-778 (2020). DOI: 10.1016/j.bioactmat.2020.05.008

71. G. Lan et al. “Highly Adhesive Antibacterial Bioactive Composite Hydrogels With Controllable Flexibility and Swelling as Wound Dressing for Full-Thickness Skin Healing.” Front Bioeng Biotechnol 9, 785302 (2021). DOI: 10.3389/fbioe.2021.785302

72. Davies, R, et al. “The Cytotoxicity of Kaolin towards Macrophages in Vitro.” British Journal of Experimental Pathology, U.S. National Library of Medicine, Aug. 1984, https://www.ncbi.nlm.nih.gov/pmc/articles/PMC2040988/.

73. Y. Liang et al. “Eliminating Heat Injury of Zeolite in Hemostasis via Thermal Conductivity of Graphene Sponge.” ACS Appl Mater Interfaces 11, 23848-23857 (2019). DOI: 10.1021/acsami.9b04956

74. Zhou, Yaping, et al. “Acetate Chitosan with Caco3 Doping Form Tough Hydrogel for Hemostasis and Wound Healing.” Polymers for Advanced Technologies 30, 143–152 (2018). DOI: 10.1002/pat.4452

75. X. Fan et al. “Tough polyacrylamide-tannic acid-kaolin adhesive hydrogels for quick hemostatic application.” Mater Sci Eng C Mater Biol Appl 109, 110649 (2020). DOI: 10.1016/j.msec.2020.110649

76. R. Pinnaratip, M. S. A. Bhuiyan, K. Meyers, R. M. Rajachar, B. P. Lee. “Multifunctional Biomedical Adhesives.” Adv Healthc Mater 8, e1801568 (2019). DOI: 10.1002/adhm.201801568

77. Y. Hong et al. “A strongly adhesive hemostatic hydrogel for the repair of arterial and heart bleeds.” Nat Commun 10, 2060 (2019). DOI: 10.1038/s41467-019-10004-7

78. J. Gao et al. “A neuroinductive biomaterial based on dopamine.” PNAS 103, 16681-16686 (2006). DOI: 10.1073pnas.0606237103

79. Cui, Haitao, et al. “4D Physiologically Adaptable Cardiac Patch: A 4-Month in Vivo Study for the Treatment of Myocardial Infarction.” Science Advances 6, (2020). DOI: 10.1126/sciadv.abb5067